Integral Constraints for Momentum and Energy in Zonal Flows with Parameterized Potential Vorticity Fluxes: Governing Parameters

V. O. IVCHENKO AND S. DANILOV

Alfred-Wegener-Institute for Polar and Marine Research, Bremerhaven, Germany

B. SINHA

National Oceanography Centre, Southampton, United Kingdom

J. SCHRÖTER

Alfred-Wegener-Institute for Polar and Marine Research, Bremerhaven, Germany

(Manuscript received 6 August 2013, in final form 4 November 2013)

ABSTRACT

Integral constraints for momentum and energy impose restrictions on parameterizations of eddy potential vorticity (PV) fluxes. The impact of these constraints is studied for a wind-forced quasigeostrophic two-layer zonal channel model with variable bottom topography. The presence of a small parameter, given by the ratio of Rossby radius to the width of the channel, makes it possible to find an analytical/asymptotic solution for the zonally and time-averaged flow, given diffusive parameterizations for the eddy PV fluxes. This solution, when substituted in the constraints, leads to nontrivial explicit restrictions on diffusivities. The system is characterized by four dimensionless governing parameters with a clear physical interpretation. The bottom form stress, the major term balancing the external force of wind stress, depends on the governing parameters and fundamentally modifies the restrictions compared to the flat bottom case. While the analytical solution bears an illustrative character, it helps to see certain nontrivial connections in the system that will be useful in the analysis of more complicated models of ocean circulation. A numerical solution supports the analytical study and confirms that the presence of topography strongly modifies the eddy fluxes.

1. Introduction

Eddies are omnipresent in the ocean, with the local maximum of energy on the mesoscale (Kamenkovich et al. 1986). Eddies redistribute momentum, and in large areas of the ocean [notably the Antarctic Circumpolar Current (ACC)] they can increase the kinetic energy of the mean flow (negative viscosity) and play an important role in the downward transport of momentum by inviscid interfacial form stress.

Numerical models either have to resolve eddies or parameterize them. Although eddy-resolving models are becoming increasingly common [e.g., Delworth et al. (2012) employ a coupled ocean–atmosphere model with unprecedented horizontal resolution in the ocean from 8 km at high latitudes to 28 km in the tropics], it is still too costly to run global eddy-resolving models over the large time periods (decades and centuries) required for climatological studies. Therefore, coarse models are used in which eddy effects are parameterized. Correct parameterizations must be based on clear physics and satisfy some basic principles: this is not always the case for some commonly used schemes. It is well known that "...the [eddy] diffusion model does not satisfactorily describe the eddy [heat, momentum or vorticity] terms..." (Harrison 1978) and that harmonic/biharmonic operators of velocity (temperature and salinity) are used for numerical stability rather than for their realism (Killworth 1997).

Green (1970) and Welander (1973) were the first to propose using parameterizations for eddy fluxes of potential vorticity (PV). This idea was implemented in a number of recent studies (Wardle and Marshall 2000; Eden and Greatbatch 2008; Eden 2010; Marshall and

Corresponding author address: V. O. Ivchenko, Alfred Wegener Institute for Polar and Marine Research, P.O. Box 12 01 61, 27515 Bremerhaven, Germany.
E-mail: vladimir.ivchenko@awi.de

DOI: 10.1175/JPO-D-13-0173.1

Adcroft 2010; Ringler and Gent 2011). However, the coefficients in these parameterizations cannot be selected arbitrarily, as there are integral constraints that have to be satisfied. The importance of integral constraints for the flat bottom case was demonstrated in Marshall (1981), Ivchenko (1984), Ivchenko et al. (1997), Olbers (2005), and Ivchenko et al. (2008). Recognizing the role of constraints, Marshall et al. (2012) propose a framework for parameterizing eddy potential vorticity fluxes that is consistent with conservation of energy and momentum while retaining the symmetries of the original eddy flux. The outstanding question of how variable bottom topography modifies the integral constraints and affects the parameterization coefficients has not been fully addressed by previous studies dealing with the parameterization of eddy PV fluxes. The generalized theorem of Bretherton (GTB), expressing the constraint on momentum in a channel with variable bottom topography, was proven by Ivchenko (1987), and Ivchenko et al. (2013) were the first to apply this constraint. However, it is not the only constraint, and parameterizations of PV fluxes have to satisfy additional requirements among which are the other integral constraints—the energy inequality (EI) and the eddy quasigeostrophic (QG) potential enstrophy inequality.[1] The latter is automatically satisfied if the coefficient of quasigeostrophic potential vorticity (QPV) diffusivity (CPV) is not negative (Ivchenko et al. 1997). The EI constraint has not been applied for the case with variable bottom topography. This paper extends previous studies and seeks

- To prove the energy inequality and study its impact on admissible PV diffusivities in a zonal channel with variable bottom topography;
- To extend previous results pertaining to how the integral constraint for momentum (GTB) affects the parameterization in a zonal channel with complex bottom topography when the zonal-mean anomaly of bottom topography differs from zero [in contrast to Ivchenko et al. (2013)];
- To determine how the PV diffusivities constrained by the GTB and EI and the bottom form stress (BFS) respond to the governing parameters; and
- To develop a simple expression linking the mean zonal transport to the governing parameters.

We achieve these aims by considering a simplified time- and zonally averaged ocean, in a channel configuration, with sinusoidal bottom topography. We parameterize the eddy transport of potential vorticity as a diffusive process with unknown diffusion coefficients. This system is simple enough to be solvable analytically. The analytical solution thus gives us the flow field (zonal velocities, etc.) in terms of the unknown diffusion coefficients. We then substitute the analytical solution into mathematical expressions for the integral constraints introduced above (generalized theorem of Bretherton and energy inequality). This process results in some very interesting and useful restrictions on the size of the diffusion coefficients, their variation with depth, and their dependence on external parameters such as the height of the bottom topography.

We consider quasigeostrophic dynamics in a two-layer fluid driven by winds over an uneven bottom. This is a major simplification of the real dynamics and is used here as a conceptual tool, allowing us to make the problem analytically tractable and to illustrate the interaction between the parameterizations and the flow dynamics. We use numerical simulations to demonstrate qualitative agreement of conclusions derived analytically with the full solution.

The analytical solution is facilitated by the smallness of the relative vorticity in zonal channels compared to the planetary vorticity or the ''stretching term'' in the expression for the QPV. The order of the differential equation is set by the relative vorticity term, so that the equations have a small parameter at the highest derivative leading to thin boundary layers near the walls. The small parameter γ is the ratio of the Rossby radius to the width of the channel. Its presence allows us to use the technique of asymptotic expansion in this parameter.

The paper is organized as follows: We first write down the main equations (fluid flow and integral constraints) and discuss the analytical solution (sections 2 and 3). Although its derivation was presented by Ivchenko et al. (2013), we briefly recapitulate it for convenience, putting details in the appendix. Section 4 discusses how the energy and momentum constraints shape the behavior of the diffusivities. Zonal momentum redistribution by eddies and net zonal transport in the presence of topography is the subject of section 5. Section 6 describes a numerical model used for simulations and presents a comparison with results found with the analytical model. Section 7 consists of a discussion of the results and conclusions.

2. Basic quasigeostrophic equations for the zonal channel and general constraints

a. Equations

We use the quasigeostrophic equations for a two-layer model (McWilliams et al. 1978):

[1] Note that there are other constraints, arising from local limitations on the amplitude of eddy stresses, as suggested by Marshall et al. (2012).

$$\frac{\partial q_1}{\partial t} + J(\Psi_1, q_1) = \frac{1}{H_1}\mathrm{curl}_z \boldsymbol{\tau} + F_1 \quad \text{and} \tag{1}$$

$$\frac{\partial q_2}{\partial t} + J(\Psi_2, q_2) = -\epsilon \mathrm{curl}_z \mathbf{v}_2 + F_2, \tag{2}$$

where q_i and Ψ_i are quasigeostrophic potential vorticity and streamfunction, respectively; subscripts mark the layers of constant mean thicknesses H_i and $\boldsymbol{\tau}$ is the wind stress divided by the water reference density. The fluid velocity $\mathbf{v}_i = (u_i, v_i)$ is expressed as $u_i = -\partial\Psi_i/\partial y$ and $v_i = \partial\Psi_i/\partial x$ in the zonal and meridional directions, respectively. Lateral friction F_i is biharmonic in the numerical simulations but is omitted in the analytical solution and

$$J(A, B) = -\frac{\partial A}{\partial y}\frac{\partial B}{\partial x} + \frac{\partial A}{\partial x}\frac{\partial B}{\partial y}$$

is the Jacobian operator, and ϵ is the linear bottom drag.

The layerwise quasigeostrophic potential vorticities q_i are given by

$$q_1 = \nabla^2\Psi_1 + f - \frac{f_0^2}{g' H_1}(\Psi_1 - \Psi_2) \quad \text{and} \tag{3}$$

$$q_2 = \nabla^2\Psi_2 + f + \frac{f_0^2}{g' H_2}(\Psi_1 - \Psi_2) + \frac{f_0}{H_2}B, \tag{4}$$

where $g' = g\rho_0^{-1}(\rho_2 - \rho_1)$ is the reduced gravity; g is the acceleration due to gravity; ρ_i is the density of layer i; ρ_0 is the reference density; f and f_0 denote the Coriolis parameter and its reference value, respectively; and B is the deviation of bottom topography from the constant depth of $H = H_1 + H_2$.

We derive analytical solutions for the time and zonal mean of Eqs. (1)–(4):

$$\frac{\partial \overline{q}_1}{\partial t} = 0 = -\frac{\partial}{\partial y}\overline{v_1' q_1'} - \frac{1}{H_1}\frac{\partial}{\partial y}\overline{\tau}_x + \overline{F_1}, \tag{5}$$

$$\frac{\partial \overline{q}_2}{\partial t} = 0 = -\frac{\partial}{\partial y}\overline{v_2' q_2'} + \epsilon\frac{\partial}{\partial y}\overline{u_2} + \overline{F_2}, \tag{6}$$

$$\overline{q}_1 = -\frac{\partial}{\partial y}\overline{u}_1 + f - \frac{f_0^2}{g' H_1}(\overline{\Psi}_1 - \overline{\Psi}_2), \quad \text{and} \tag{7}$$

$$\overline{q}_2 = -\frac{\partial}{\partial y}\overline{u}_2 + f + \frac{f_0^2}{g' H_2}(\overline{\Psi}_1 - \overline{\Psi}_2) + \frac{f_0}{H_2}\overline{B}. \tag{8}$$

The overbar here denotes the time and zonal average, and the prime implies the eddy component, that is, the deviation from the time and zonal mean.

To proceed further, we assume a diffusive parameterization for eddy fluxes of QPV in each layer,

$$\overline{v_i' q_i'} = -K_i\frac{\partial \overline{q}_i}{\partial y}, \quad \text{for} \quad i = 1, 2, \tag{9}$$

where $K_i \geq 0$ is the respective CPV. In doing so we follow numerous studies (Taylor 1915; Green 1970; Rhines 1977; Marshall 1981; Killworth 1997; Treguier et al. 1997; Wardle and Marshall 2000; and others) proposing that the eddy transfer of PV is downgradient. The presence of a rotational component in eddy fluxes and problems with its separation (Fox-Kemper et al. 2003) add complexity to this problem. However, we think that the downgradient assumption of eddy PV flux presents an appropriate starting point. These parameterizations, when substituted into Eqs. (5)–(6), will lead to a closed set of equations that can be solved for any K_i. The point, however, is that the solutions should satisfy certain integral constraints, which in turn restrict the admissible values for K_i. As pointed out by Ivchenko et al. (2013), the GTB presents one such constraint, which immediately imposes a link between the layer diffusivities K_1 and K_2. We shall analyze it in more detail here and also take into account additional constraints as explained below.

b. Generalized theorem of Bretherton

We begin by noting that the integration of the time- and zonal-mean potential vorticity Eqs. (5)–(6) in the meridional direction for a stationary regime, disregarding horizontal friction, yields

$$\overline{v_1' q_1'} = -H_1^{-1}\tau_x \quad \text{and} \tag{10}$$

$$\overline{v_2' q_2'} = \epsilon\overline{u_2}, \tag{11}$$

where the constants of integration in Eqs. (10)–(11) are set to zero because the eddy fluxes, wind stress, and zonal-mean velocity are enforced as zero on the solid boundaries in our solutions (Marshall 1981; Ivchenko et al. 2013).

Combining Eqs. (10)–(11) we find

$$H_1\overline{v_1' q_1'} + H_2\overline{v_2' q_2'} = -\tau_x + H_2\epsilon\overline{u_2}. \tag{12}$$

This expression is valid for arbitrary bottom topography. For a flat bottom channel, the meridional integral of the left-hand side of Eq. (12) becomes zero according to the Bretherton theorem (Taylor 1915; Bretherton 1966; McWilliams et al. 1978; Marshall 1981; Ivchenko et al. 2013):

$$\int_0^L (H_1\overline{v_1'q_1'} + H_2\overline{v_2'q_2'})\,dy = 0. \tag{13}$$

Hence, for the flat bottom channel, the main force by wind stress is balanced by the bottom drag:

$$\int_0^L (\tau_x - H_2\epsilon\overline{u_2})\,dy = 0. \tag{14}$$

It is well known that this balance, valid in the absence of bottom topography, results in an unrealistically high transport of the ACC (Munk and Palmén 1951) if applied in the Southern Ocean.

Substitution of the diffusive parameterization, Eq. (9), in the Bretherton theorem, Eq. (13), yields

$$\int_0^L \left(K_1H_1\frac{\partial\overline{q_1}}{\partial y} + K_2H_2\frac{\partial\overline{q_2}}{\partial y}\right) dy = 0. \tag{15}$$

This expression relates to the first instability criterion of Pedlosky: ''the potential vorticity gradient must be somewhere positive and somewhere negative for instability to occur'' (Pedlosky 1964).

For variable bottom topography the Bretherton theorem is replaced by the GTB (Ivchenko 1987; Ivchenko et al. 2013):

$$\int_0^L (H_1\overline{v_1'q_1'} + H_2\overline{v_2'q_2'})\,dy = f_0\int_0^L \overline{v_2B}\,dy. \tag{16}$$

The term within the integral on the rhs of Eq. (16) is the bottom form stress, since

$$f_0\overline{v_2B} = -\overline{p_2\frac{\partial B}{\partial x}}, \tag{17}$$

where p_2 is the pressure in the lower layer normalized by the reference density.

The bottom form stress is an inviscid mechanism that redistributes momentum. We cannot expect acceleration of the zonal flow by this mechanism, which yields

$$f_0\int_0^L \overline{v_2B} < 0. \tag{18}$$

This can be used, in addition to the GTB, as an extra constraint the solution has to satisfy.

Again, we can substitute the diffusive parameterization of eddy QPV fluxes given by Eq. (9) into the GTB, Eq. (16), to obtain

$$\int_0^L \left(K_1H_1\frac{\partial\overline{q_1}}{\partial y} + K_2H_2\frac{\partial\overline{q_2}}{\partial y}\right) dy = -f_0\int_0^L \overline{v_2\,B}\,dy. \tag{19}$$

Because of Eq. (18) the rhs of Eq. (19) is positive, and instability (more accurately, states with nonzero eddy kinetic energy) in a channel with variable bottom topography can occur even if the potential vorticity gradient is everywhere positive, in contrast to the flat bottom case.

Eddies redistribute the mean zonal momentum, and following Pedlosky (1964, 1979) and using Eq. (12) this balance can be written

$$\frac{\partial}{\partial t}(H_1\overline{u_1} + H_2\overline{u_2}) = 0 = (H_1\overline{v_1'q_1'} + H_2\overline{v_2'q_2'}) + \tau_x - H_2\epsilon\overline{u_2}. \tag{20}$$

The first term on the right-hand side of Eq. (20) therefore describes the redistribution of zonal barotropic momentum by eddies.

If we substitute the GTB, Eq. (16), into the meridionally integrated momentum balance Eq. (12), we find that the wind stress is balanced by the bottom friction and the bottom form stress:

$$\int_0^L \tau_x\,dy - \int_0^L H_2\epsilon\overline{u_2}\,dy + f_0\int_0^L \overline{v_2B}\,dy = 0. \tag{21}$$

The second term on the left-hand side is commonly much smaller than the wind stress term in the presence of topography, and the balance is between the wind stress and bottom form stress both for a zonal channel with an uneven bottom and the ACC (Munk and Palmén 1951; Ivchenko et al. 1996; Stevens and Ivchenko 1997).

Numerical experiments show that even a small zonal variation in B substantially reduces the zonal transport (McWilliams et al. 1978; Treguier and McWilliams 1990; Sinha and Richards 1999; Wolff et al. 1991). We therefore expect that the link between the diffusivities will be affected by the presence of bottom topography.

c. Energy inequality

By multiplying the instantaneous quasigeostrophic potential vorticity [Eqs. (1)–(2)] by $H_i\Psi_i'$, taking the time and zonal average, summing layer contributions, and integrating in the meridional direction, we obtain the budget of the total eddy mechanical (i.e., kinetic and available potential) energy. The balance is expressed as

$$\frac{\partial}{\partial t}\int_0^L (\mathrm{KE}_1^{\mathrm{ed}} + \mathrm{KE}_2^{\mathrm{ed}} + \mathrm{APE}^{\mathrm{ed}})\,dy = 0 = -\int_0^L (H_1\overline{u_1v_1'q_1'} + H_2\overline{u_2v_2'q_2'})\,dy - \int_0^L \{H_1\overline{F_1'\Psi_1'} + H_2\overline{F_2'\Psi_2'} + H_2\epsilon[\overline{(u_2')^2} + \overline{(v_2')^2}]\}\,dy, \tag{22}$$

where KE_1^{ed}, KE_2^{ed}, and APE^{ed} are the eddy kinetic energy for the upper and lower layers and the eddy available potential energy, respectively (Ivchenko 1987; Ivchenko et al. 1997). We assume that the wind is steady and zonally uniform, depending only on the meridional coordinate.

The first term on the right-hand side corresponds to the generation of total eddy mechanical energy by baroclinic and/or barotropic instabilities. The second term on the right-hand side contains dissipation terms due to the horizontal and bottom friction. For steady-state solutions, the eddy mechanical energy is positive only if the generation term is positive:

$$\int_0^L (H_1\overline{u_1'v_1'q_1'} + H_2\overline{u_2'v_2'q_2'})\,dy < 0. \tag{23}$$

Once again, using the diffusive parameterization of eddy QPV fluxes, Eqs. (9) and (23) can be rewritten in the form

$$\int_0^L \left(K_1H_1\overline{u_1}\frac{\partial\overline{q_1}}{\partial y} + K_2H_2\overline{u_2}\frac{\partial\overline{q_2}}{\partial y}\right)dy > 0. \tag{24}$$

This statement agrees with the second instability condition of Pedlosky: ''the product of the zonal velocity and the potential vorticity gradient must in all cases be somewhere positive for instability to occur'' (Pedlosky 1964). In the context of this study, it is this constraint on the solutions with parameterized eddy fluxes that leads to further restrictions on the diffusivities. Clearly, all the constraints discussed thus far (the GTB, negativity of the form stress, and the energy inequality) are not independent, yet lead to different limitations.

3. Analytical solution

We set the wind stress to be zonal and to vary as the sine of the meridional coordinate:

$$\tau_x = \tau_0 \sin(\pi y L^{-1}), \tag{25}$$

where τ_0 is the amplitude of zonal wind stress. We also prescribe the bottom topography deviation B as

$$B = B_0 \sin(2\pi y L^{-1})[\sigma + \sin(2k\pi x L_x^{-1})], \tag{26}$$

where B_0 is the amplitude of bottom topography and σ is a nondimensional parameter. If $\sigma \neq 0$, the zonal-mean deviation of bottom topography is not zero, but remains a function of the meridional coordinate. Other than this, the topography selected is zonally periodic and takes zero values at the meridional boundaries ($y = 0, L$). We substitute Eq. (9) in the time and zonally averaged equations for QPV [Eqs. (5)–(6)], omit the lateral friction, and rewrite them in dimensionless form (Marshall 1981; Ivchenko 1987; Ivchenko et al. 2013):

$$\gamma\frac{\partial}{\partial y^*}\left(s_1\frac{\partial q_1^*}{\partial y^*}\right) - \frac{u_s}{u_c}\cos(\pi y^*) = 0 \quad \text{and} \tag{27}$$

$$\gamma\frac{\partial}{\partial y^*}\left(s_2\frac{\partial q_2^*}{\partial y^*}\right) + \epsilon^*\frac{\partial u_2^*}{\partial y^*} = 0, \tag{28}$$

where the asterisk marks dimensionless variables $y = Ly^*$, $\Psi_i = Lu_c\Psi_i^*$, $\overline{q_i} = \beta L q_i^*$, and $\overline{u}_i = u_c u_i^*$. We also introduce the following parameters $\delta_i = H_i H^{-1}$, $\gamma = L_R L^{-1}$, $L_R = (g'H_1H_2f_0^{-2}H^{-1})^{1/2}$, $\epsilon = \beta L\epsilon^*$, and the dimensionless CPVs $s_i = K_i(L_R u_c)^{-1}$. The wind amplitude enters through $u_s = (\pi\tau_0)(H_1\beta L)^{-1}$, and $u_c = g'\beta H f_0^{-2}$ is the channel velocity scale, chosen so that the stretching term in QPV balances the meridional variation in planetary vorticity (Marshall 1981).

We are interested in obtaining an analytical solution to Eqs. (27)–(28), applying boundary conditions of no flux through the solid boundaries:

$$\overline{v_i'q_i'}|_{0,L} = 0. \tag{29}$$

The procedure of solution is similar to that of Ivchenko et al. (2013), except for the addition of the parameter σ to the topography anomaly (with respect to the reference depth H). We assume the coefficients K_i (s_i) to be constant over the channel, except for two thin boundary layers near the walls with thickness $\Delta \ll 1$, where they are linearly reduced to zero, which allows us to satisfy boundary conditions.

Solving equations and analyzing solutions in nondimensional form offers some advantages, simplifying the use of the asymptotic expansion technique (see below) and introducing nondimensional parameters that reflect the main balances between the terms in the governing equations. However, a caveat is that nondimensional parameters can be dependent on several physical parameters, which should be kept in mind in the analysis. The system [Eqs. (27)–(28)] contains a small parameter $\gamma = L_R L^{-1}$. Its presence allows us to apply an asymptotic expansion in this parameter and match solutions in the boundary layers with the solution outside them. The mathematical details of this technique are the same as in Ivchenko et al. (2013). For convenience, they are repeated in the appendix. The solutions for the zonal velocities are given by Eqs. (A15)–(A18), in the appendix. From these we are able to obtain expressions for potential vorticities and streamfunctions in each layer, and from the latter we can obtain the meridional

velocity in order to calculate the bottom form stress. After solutions are found, they are substituted in the constraints discussed above, enabling us to analyze the limitations on CPV as a function of model parameters.

4. Results: Integral constraints

In this section we substitute the analytic solution derived in the appendix [Eqs. (A15)–(A18)] into the GTB and energy inequality, given, respectively, by Eqs. (16) and (24) of section 2. Since the analytic solutions are functions of the layerwise CPVs, we thus obtain a set of restrictions on the CPVs that depend on the governing parameters. The impact of these restrictions on the CPVs and the behavior of the BFS are illustrated by Figs. 1–5.

a. Integral constraint for momentum (GTB)

The GTB, given by Eq. (19), can be written in dimensionless form as

$$\int_0^1 \left(\delta_1 s_1 \frac{\partial q_1^*}{\partial y^*} + \delta_2 s_2 \frac{\partial q_2^*}{\partial y^*}\right) dy^* = \frac{f_0 S}{H L_R u_c \beta} \int_0^1 \overline{v_2 B}^*\, dy^*, \tag{30}$$

where S is the scaling of $\overline{v_2 B}$, that is,

$$\overline{v_2 B} = S \overline{v_2 B}^*, \tag{31}$$

and v_2 is obtained from Ψ_2 [see appendix Eq. (A6)].

Substituting solutions for the meridional gradients of QPV and bottom form stress into Eq. (30), we obtain

$$\begin{aligned} &12D + 6\pi^2 \alpha_B \alpha_U - 12\delta_1 \,\mathrm{Re}\alpha_B \alpha_U \\ &\quad = 8\delta_1 \,\mathrm{Re}\alpha_B \alpha_T \alpha_U - 3\pi^2 \alpha_B \alpha_T \alpha_U - 3\sigma\pi^3 \delta_2 \alpha_B \alpha_R \alpha_T \alpha_U. \end{aligned} \tag{32}$$

Equation (32) introduces two nondimensional parameters involving the CPVs. These are $\mathrm{Re} = u_s L K_1^{-1}$, which is an analog of the Reynolds number, and $D = \epsilon u_c (\beta K_2)^{-1}$, which characterizes the relation between the bottom friction and diffusion of QPV in the lower layer.

Four other nondimensional parameters α_B, α_R, α_T, and α_U are now introduced:

$$\alpha_B = \frac{L_R u_c}{\delta_1 u_s L}, \tag{33}$$

$$\alpha_R = \frac{|f_0| B_0}{L H_2 \beta}, \tag{34}$$

$$\alpha_T = \frac{B_0 L |f_0||b|k}{H L_x \delta_2 \epsilon}, \quad \text{and} \tag{35}$$

$$\alpha_U = \frac{\epsilon}{\beta L_R}. \tag{36}$$

The parameter α_B^{-1} estimates the relative importance of wind stress and the stretching term in the meridional gradient of QPV for the upper layer. The parameter α_R measures the ratio between the "topographic" $(|f_0|B_0)H_2^{-1}$ and planetary βL contributions to the QPV in the lower layer. The physical sense of parameter α_T is the relative importance of inviscid bottom form stress against viscous bottom friction. Finally, the parameter α_U is the ratio between the time scale of zonal baroclinic Rossby waves and that of dissipation by bottom friction. Two of these parameters (α_B and α_U) depend on the stratification, amplitude of wind stress, bottom friction, β, Rossby radius, and other parameters, but do not directly involve the characteristics of topography. We will call them the "flow parameters." The two remaining parameters (α_R and α_T) depend on the amplitude of bottom topography deviation and will be referred to as the "topographic parameters." We apply our theory for the Southern Hemisphere, where $f_0 < 0$.

Equation (32) can be rewritten for D as a linear function of Re:

$$D = M_1 \,\mathrm{Re} + M_2, \tag{37}$$

where

$$M_1 = \left(\frac{2}{3}\delta_1 \alpha_B \alpha_T \alpha_U + \delta_1 \alpha_B \alpha_U\right) \quad \text{and} \tag{38}$$

$$\begin{aligned} M_2 = &-\frac{1}{2}(\pi^2 \alpha_B \alpha_U) - \frac{1}{4}(\pi^2 \alpha_B \alpha_T \alpha_U) \\ &- \frac{1}{4}(\pi^3 \delta_2 \alpha_B \alpha_R \alpha_T \alpha_U \sigma). \end{aligned} \tag{39}$$

Although the relationship between D and Re is linear, the relationship between K_2 and K_1 is nonlinear. Since $\mathrm{Re} > 0$ and $D > 0$, Eq. (37) yields a critical value $\mathrm{Re}_{\mathrm{cr}}$:

$$\mathrm{Re} > \mathrm{Re}_{\mathrm{cr}} = -\frac{M_2}{M_1} = \frac{6\pi^2 + 3\pi^2 \alpha_T + 3\pi^3 \delta_2 \alpha_R \alpha_T \sigma}{8\delta_1 \alpha_T + 12\delta_1}. \tag{40}$$

This immediately implies that there is an upper bound on the CPV of the upper layer. Note, that $\mathrm{Re}_{\mathrm{cr}} > 0$ exists even for the flat bottom channel (Ivchenko et al. 1997), which means that if $\mathrm{Re} < \mathrm{Re}_{\mathrm{cr}}$ the flow is not unstable for baroclinic instability.

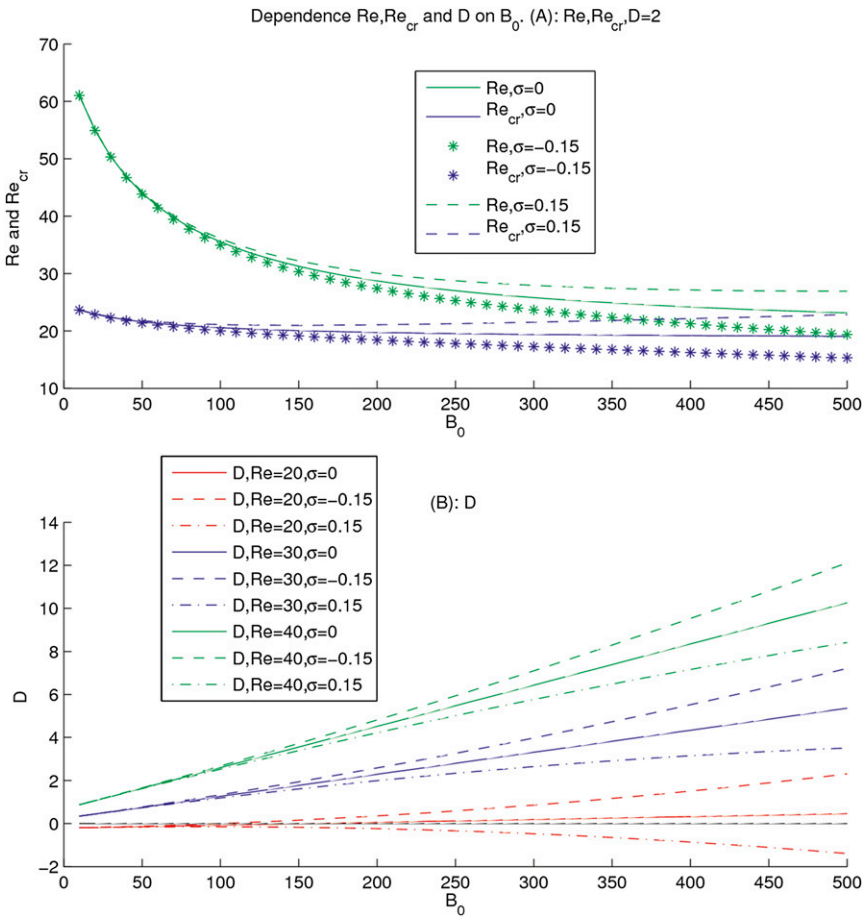

FIG. 1. (a) Re (green) and $\mathrm{Re_{cr}}$ (blue) versus B_0, with $D = 2$. (b) D versus B for Re = 20 (red), 30 (blue), and 40 (green). In both panels $\sigma = 0$ (solid), -0.15 (asterisks), and 0.15 (dashed).

The values of Re and $\mathrm{Re_{cr}}$ decrease nonlinearly when the amplitude of B_0 is increased (Fig. 1a). For fixed Re, the value of D increases if the amplitude B_0 is increased for physically meaningful solutions (see Fig. 1b). If B_0 is small and Re insufficiently high, the parameter D could became negative, which is forbidden. For larger prescribed Re, D increases accordingly. The relationship $D(B_0)$ is linear for fixed Re if $\sigma = 0$ and weakly nonlinear if $\sigma \neq 0$. For subsequent calculations we use the following set of ''standard'' values: $u_s = 1.5 \times 10^{-2}\,\mathrm{m\,s^{-1}}$, $u_c = 1.4 \times 10^{-1}\,\mathrm{m\,s^{-1}}$, $L = 1.5 \times 10^{6}\,\mathrm{m}$, $L_x = 8 \times 10^{6}\,\mathrm{m}$, $H_1 = 10^{3}\,\mathrm{m}$, $H_2 = 4 \times 10^{3}\,\mathrm{m}$, $k = 4$, $b = -0.16$, $\epsilon = 10^{-7}\,s^{-1}$, $\beta = 1.4 \times 10^{-11}\,\mathrm{m^{-1}\,s^{-1}}$, $\tau_0 = 10^{-4}\,\mathrm{m^2\,s^{-2}}$, and $L_R = 4 \times 10^{4}\,\mathrm{m}$ (Marshall 1981; Ivchenko et al. 2013).

In a flat bottom channel, Re = 69.6 and $\mathrm{Re_{cr}} = \pi^2(2\delta_1)^{-1} = 24.7$ for a prescribed value of $D = 2$ (Fig. 2a). If the bottom topography amplitude B_0 is varied between 0 and 500 m, for $D = 2$, and parameter $\sigma = \pm 0.15$, the critical value $\mathrm{Re_{cr}}$ is greater than 15. Positive (negative) values of σ yields higher (lower) values of $\mathrm{Re_{cr}}$ (see Fig. 2b). This happens because a negative σ provides a negative contribution to the mean meridional QPV gradient in the lower layer in the central part of the channel, $1/4 < y^* < 3/4$, where the wind forcing is strongest [see Eq. (A2)]. Since baroclinic instability plays a dominant role and the onset of instability requires a change in the sign of the mean meridional QPV gradients between the layers, and since this gradient is positive in the upper layer [see Eq. (A1)], the instability occurs for a smaller value of the mean vertical shear in the case of negative σ, that is, smaller $\mathrm{Re_{cr}}$.

According to Eqs. (37) and (38), the slope M_1 of $\partial D/\partial \mathrm{Re}$ is always positive and increases if the amplitude of bottom topography is increased, since only the parameter α_T in Eq. (38) is linked to the bottom topography (proportional to B_0). Note that the slope $\partial D/\partial \mathrm{Re}$ is independent of the parameter α_R and the ''geometric'' parameter σ. For the flat bottom case, the slope [Eq. (38)] reduces to

$$\partial D/\partial \mathrm{Re} = \delta_1 \alpha_B \alpha_U, \tag{41}$$

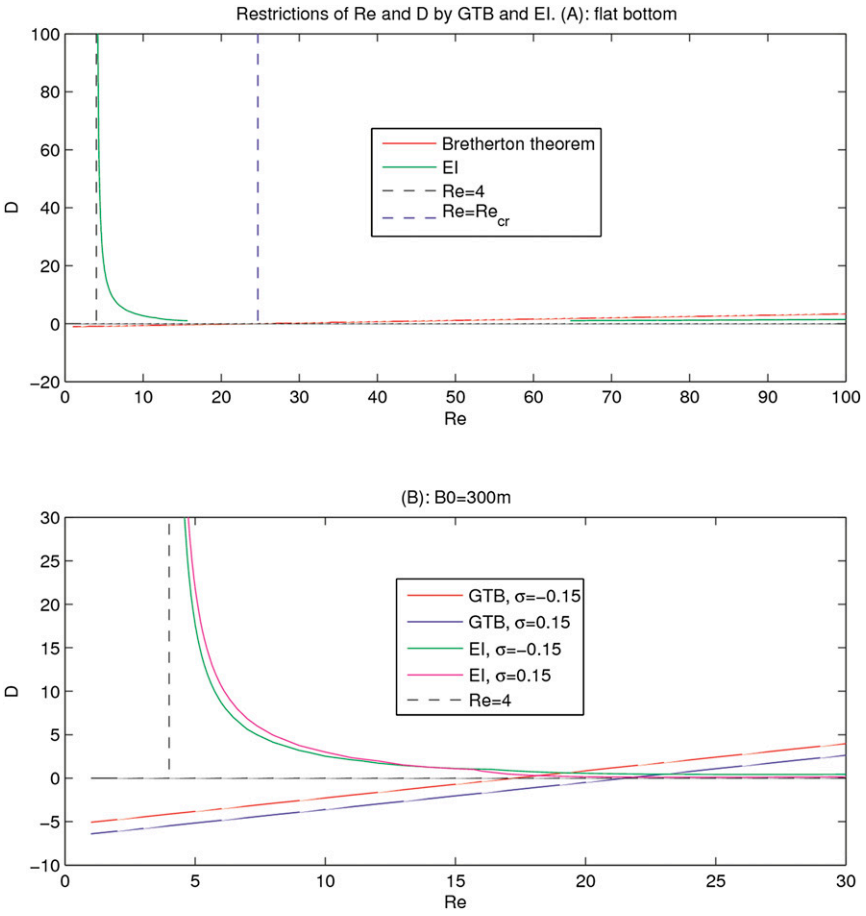

FIG. 2. Constraints of Re and D by GTB and EI for (a) flat bottom. (b) $B_0 = 300$ m. Permissible values of Re and D based on the EI lie above the corresponding curves and D must be positive.

that is, it becomes proportional to the two flow parameters.

b. *Bottom form stress: Physical mechanism and dependence on parameters*

Since the BFS plays a major role in zonal currents, like the ACC, it is important to understand what affects it and what restrictions it imposes.

The bottom form stress (i.e., the right-hand side of the GTB) can be written in dimensionless form (for the Southern Hemisphere) as

$$\mathrm{BFS} = \frac{|f_0|\int_0^L \overline{v_2 B}\, dy}{u_s \beta L^2 H} = \frac{\delta_1 \alpha_B \alpha_T \alpha_U}{6\pi^2 D}(8\delta_1\,\mathrm{Re} - 3\pi^2 - 3\sigma\pi^3\delta_2\alpha_R). \qquad (42)$$

All the parameters in the rhs before the expression in parentheses are positive, so that the inequality [Eq. (18)] is satisfied if

$$\mathrm{Re} > \frac{3\pi^2 + 3\sigma\pi^3\delta_2\alpha_R}{8\delta_1}. \qquad (43)$$

It is natural that the rhs of Eq. (43) is independent of the "topographic" parameter α_T (since it includes friction). It depends, however, on the geometric parameter σ. In the center of the channel, the meridional gradient of zonally averaged bottom topography is positive for $\sigma < 0$ and negative for $\sigma > 0$ that modifies the planetary part of QPV gradient. The respective contribution in the expression for $\partial q_2^*/\partial y^*$ [see Eq. (A2)] is $-2\pi\alpha_R\sigma\cos(2\pi y^*)$ and is negative (positive) for negative (positive) σ, which yields decreasing (increasing) total eddy QPV and accordingly BFS.

The expression for the BFS [Eq. (42)] can be rewritten by using the GTB [Eq. (37)]:

$$\mathrm{BFS} = \frac{4\delta_1\alpha_T}{\pi^2(2\alpha_T+3)} + \frac{1}{D}\frac{\delta_1\alpha_B\alpha_U\alpha_T(1-3\delta_2\pi\alpha_R\sigma)}{2(2\alpha_T+3)}. \qquad (44)$$

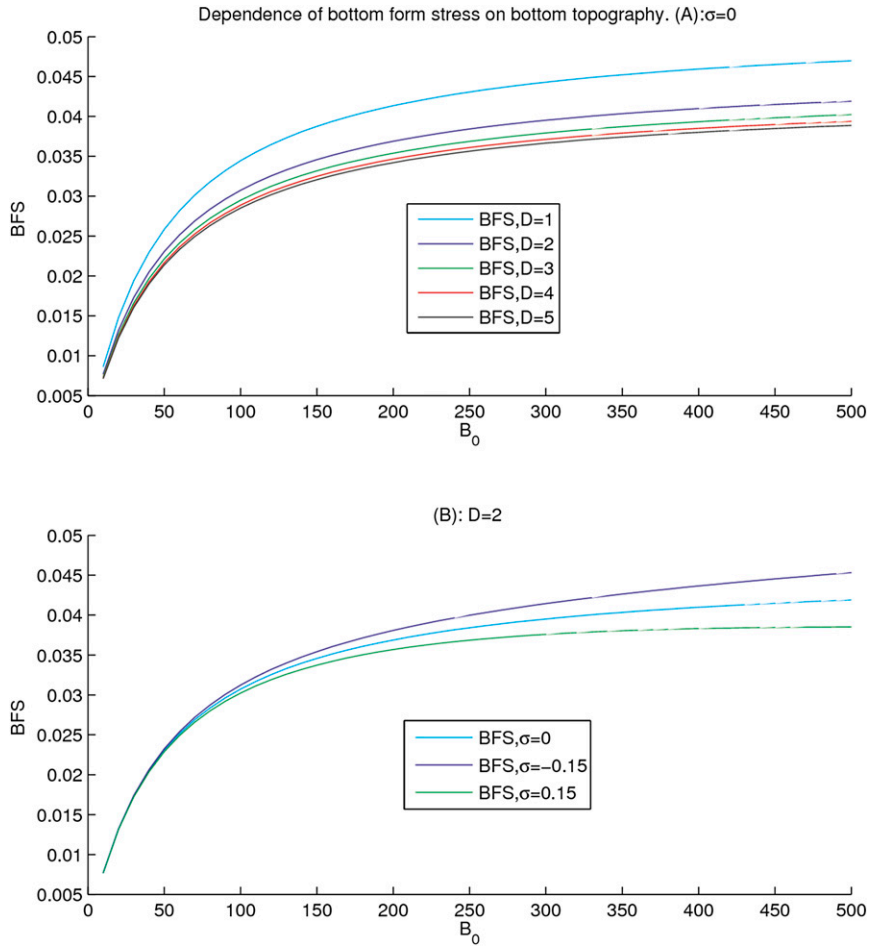

FIG. 3. Dependence of BFS on bottom topography for (a) $\sigma = 0$ and (b) $D = 2$.

We conclude that

$$1 - 3\delta_2 \pi \alpha_R \sigma > 0 \tag{45}$$

should be observed if D is small to ensure that BFS > 0.

The BFS depends nonlinearly on the amplitude of the bottom topography (Fig. 3a), especially when it is small, where $B_0 < 100$ m. The BFS is higher for small values of D, and the parameter σ only weakly affects the BFS for small B_0, but leads to larger effects for higher amplitudes of bottom topography (Fig. 3b) because nondimensional BFS depends on σ only via the last term in the brackets in Eq. (42). The term in brackets, $-3\sigma\pi^3\delta_2\alpha_R$, is proportional to B_0, since $\alpha_R \sim B_0$. This leads to a small impact of σ on BFS for small values of bottom topography, which increases with increasing B_0.

To find the dependence of the BFS on Re we use Eq. (32), that is, the GTB, and rewrite the BFS as the sum of fluxes to obtain

$$\frac{\partial \mathrm{BFS}}{\partial \mathrm{Re}} = \frac{-24\delta_1^2 \alpha_T (1 - 3\delta_2 \pi \alpha_R \sigma)}{(\mathrm{Re} 8\delta_1 \alpha_T + 12\delta_1 - 6\pi^2 - 3\pi^2 \alpha_T - 3\pi^3 \delta_2 \alpha_R \alpha_T \sigma)^2}. \tag{46}$$

The denominator in Eq. (46) is positive, and the BFS is inversely proportional to Re squared if Re is sufficiently large. The sign of this link depends on the term $(1 - 3\delta_2 \pi \alpha_R \sigma)$: if $(1 - 3\delta_2 \pi \alpha_R \sigma) > 0$, then $\partial \mathrm{BFS}/\partial \mathrm{Re} < 0$. Note, that this condition is identical to Eq. (45).

The BFS increases with bottom friction ϵ for a high enough amplitude of bottom topography B_0 (see Fig. 4a). However, it is interesting to note that the BFS decreases when ϵ increases for small B_0 (e.g., $B_0 = 100$ m in our figure). For small values of B_0 the contribution of viscous bottom drag to the mean momentum balance [Eq. (21)] becomes significant, so that the contribution of the BFS gets less important with increasing bottom friction ϵ.

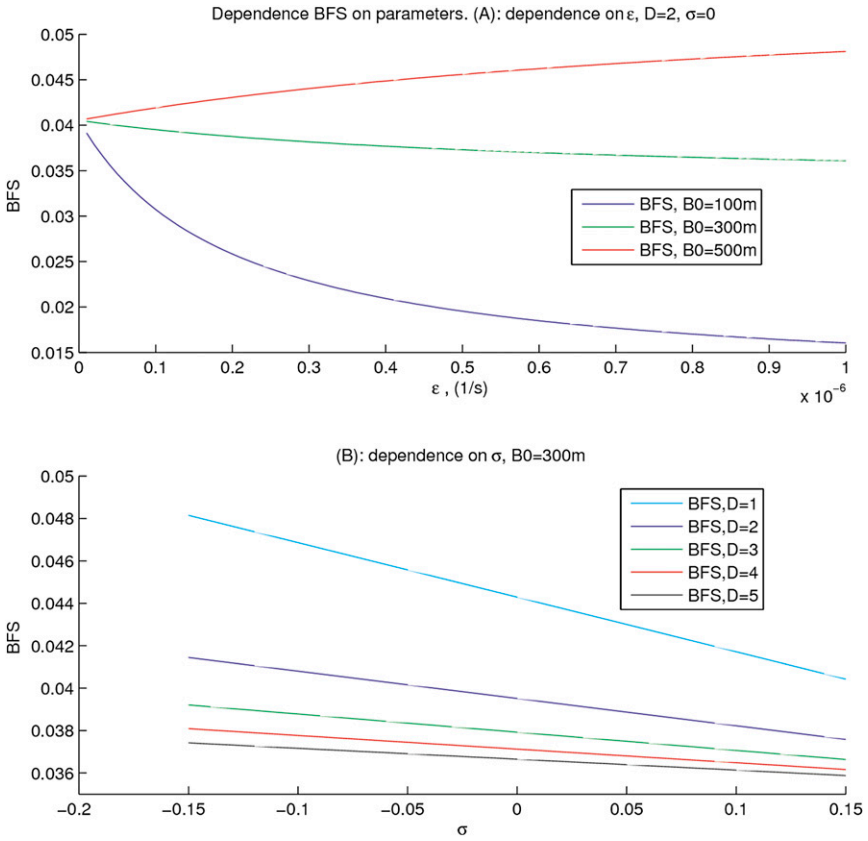

FIG. 4. Dependence of BFS on parameters (a) ϵ and (b) σ at $B_0 = 300$ m.

The BFS decreases also if the geometric parameter σ increases (Fig. 4b) or with increasing parameter D.

The value of BFS as a function of wind stress is higher for larger values of B_0 (Fig. 5a). For smaller wind stress this dependence is strongly nonlinear, but for higher wind stress it is independent of wind stress and is a function of B_0. For a high enough wind stress, the dependence of the BFS on σ is insensitive to the stress value (Fig. 5b), but for smaller values (in the range of climatological values along the ACC, i.e., about $10^{-4}\,\mathrm{m^2\,s^{-2}}$) the BFS displays nonlinear dependence on wind stress. This happens because the nondimensional BFS depends on the wind stress via two parameters: $\alpha_B \sim u_s^{-1} \sim \tau_0^{-1}$ and $\mathrm{Re} \sim u_s \sim \tau_0$, which leads to the independence of nondimensional BFS on the wind stress for large values of Re; that is, for

$$\mathrm{Re} \gg (3\pi^2 + 3\sigma\pi^3\delta_2\alpha_R)/(8\delta_1) \tag{47}$$

[see Eq. (42)]. This last condition corresponds to high values of wind stress.

c. *Integral constraint for energy*

The energy inequality [Eq. (24)] can be rewritten in dimensionless form as

$$\int_0^1 \left(\delta_1 s_1 u_1^* \frac{\partial q_1^*}{\partial y^*} + \delta_2 s_2 u_2^* \frac{\partial q_2^*}{\partial y^*}\right) dy^* > 0. \tag{48}$$

Substituting solutions for velocities [Eqs. (A15)–(A18)] and meridional gradients of QPV into this inequality we find, after some rearrangement,

$$3\delta_1\delta_2\,\mathrm{Re}D^2 + 3\delta_1\,\mathrm{Re}D - 12\delta_1\delta_2 D^2 - 12D - 8\pi\delta_2\alpha_R\sigma D + 24\delta_1\alpha_B\alpha_U\,\mathrm{Re} - 6\pi^2\alpha_B\alpha_U - 3\delta_1^2\alpha_B\alpha_U\,\mathrm{Re}^2$$
$$+ 8\pi\delta_1\delta_2\alpha_B\alpha_U\alpha_R\sigma\,\mathrm{Re} + 8\pi\delta_1\delta_2\alpha_B\alpha_U\alpha_R\sigma\,\mathrm{Re} - 12\pi^4\delta_2^2\alpha_B\alpha_U\alpha_R^2\sigma^2 > 0. \tag{49}$$

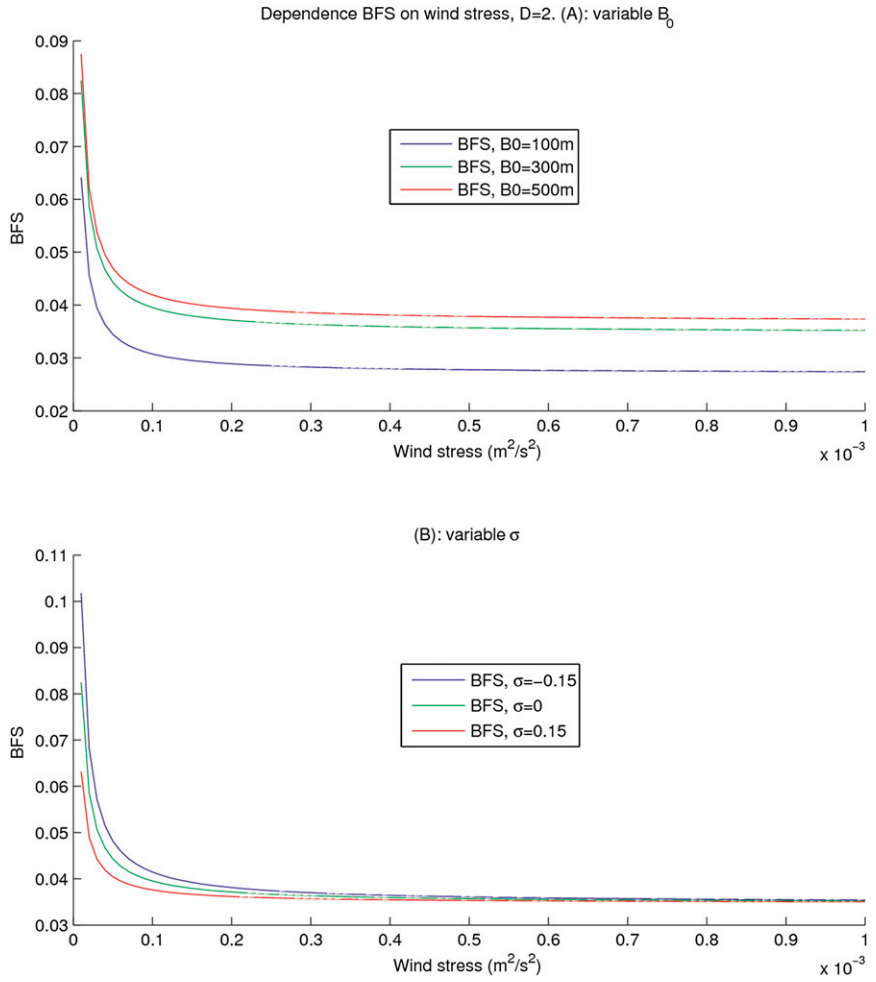

FIG. 5. Dependence of BFS on wind stress, where $D = 2$ for (a) variable B_0 and (b) variable σ.

In Eq. (49), the parameters Re and D are linked via the GTB [i.e., Eq. (37)]; this will introduce the topographic parameter α_T to the EI.

It is straightforward to find an asymptotic value of Re when D tends to infinity:

$$\lim_{D\to\infty} \mathrm{Re} = 4, \tag{50}$$

so that $\mathrm{Re} > 4$ for any set of external parameters (including the flat bottom case) (see Figs. 2a,b).

The asymptotic value of $\mathrm{Re} = 4$ corresponds to the averaged value of CPV in the upper layer:

$$K_1 < \frac{\pi\tau_0}{4H_1\beta} = 5.6\times 10^3\ \mathrm{m^2\,s^{-1}} \tag{51}$$

for the standard set of parameters.

From Eq. (49) and Figs. 2a and 2b, we can see that there are restrictions on the parameter D, but there is no asymptotic form as there is for Re.

Note that the parameter D is proportional to the bottom viscosity ϵ. This means that the limit case of $D = 0$ cannot provide a physically reasonable solution because in the presence of forcing (wind stress), the system must rely on the bottom drag to reach a stationary regime. The GTB does not exclude the zero value of D.

5. Momentum redistribution by eddies and zonal transport

Eddies redistribute zonal momentum, locally increasing or decreasing it. In this section we examine the zonal redistribution of momentum by the parameterized eddies in our analytic solution and investigate how this redistribution process is modified by the presence of topography compared to the flat bottom case. We also use our analytic solution to investigate the parameters that govern the magnitude of the net zonal transport. The results are illustrated in Figs. 6–11.

a. Momentum redistribution

We begin by considering the zonal momentum balance, Eq. (20), which can be rewritten in nondimensional form as

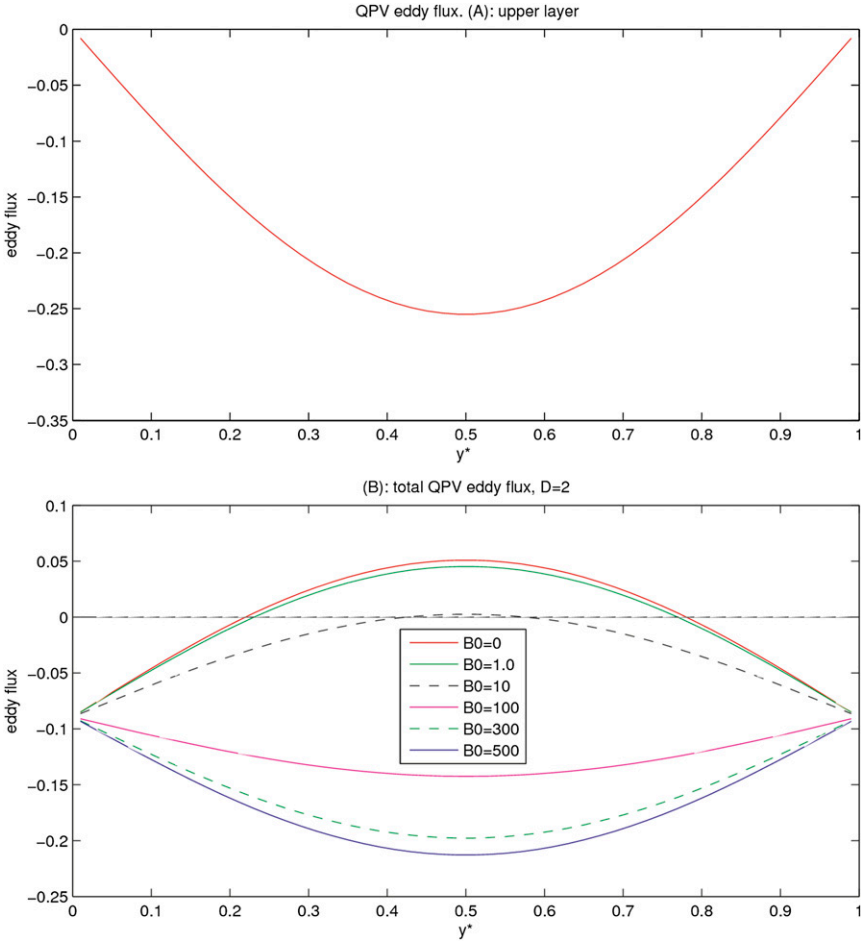

FIG. 6. QPV eddy flux for (a) upper layer and (b) total flux, with $D = 2$.

$$\frac{\partial}{\partial t^*}(\delta_1 u_1^* + \delta_2^* u_2^*) = -\frac{T_0}{T_R}\left(\frac{1}{\alpha_B \mathrm{Re}}\frac{\partial q_1^*}{\partial y^*} + \frac{\delta_2 \alpha_U}{D}\frac{\partial q_2^*}{\partial y^*}\right) + \frac{T_0}{T_R}\frac{1}{\pi\alpha_B}\sin(\pi y^*) - \frac{T_0}{T_R}\delta_2\alpha_U u_2^*, \tag{52}$$

where T_0 is the characteristic time scale of the process; that is, $t = T_0 t^*$ and $T_R = (\beta L_R)^{-1}$ is the time scale associated with a zonal baroclinic Rossby wave. The first term on the right-hand side is the eddy redistribution of momentum, the second term is the external forcing (by wind), and the last term is the bottom friction. According to Eq. (10), the eddy flux of QPV in the upper layer depends on wind stress and H_1 only (see Fig. 6a). Eddies increase the vertically integrated mean momentum when the first term on the right-hand side of Eq. (52) is positive. To find where this happens for a flat bottom channel, we use the solutions for mean zonal velocities of Eqs. (A15)–(A18) and substitute them into the expression for mean meridional gradients of the QPV [Eqs. (A1)–(A2)], which yields

$$\sin(\pi y^*)(\delta_1\alpha_B\alpha_U \mathrm{Re} - D) - \pi\alpha_B\alpha_U > 0. \tag{53}$$

Therefore from Eqs. (37)–(39) and $\delta_1\alpha_B\alpha_U\mathrm{Re} - D > 0$, the region where eddies increase the mean zonal barotropic momentum is (see Fig. 6b, red line, the region where eddy flux is greater than 0)

$$\begin{aligned}&\frac{1}{\pi}\arcsin\left(\frac{\pi\alpha_B\alpha_U}{\delta_1\alpha_B\alpha_U\mathrm{Re} - D}\right)\\ &\quad = y_1^* < y^* < y_2^*\\ &\quad = 1 - \frac{1}{\pi}\arcsin\left(\frac{\pi\alpha_B\alpha_U}{\delta_1\alpha_B\alpha_U\mathrm{Re} - D}\right).\end{aligned} \tag{54}$$

The bottom topography strongly affects the eddy redistribution of zonal momentum, especially at small amplitudes, when the flow regime changes from a flat bottom one to one where bottom form stress dominates.

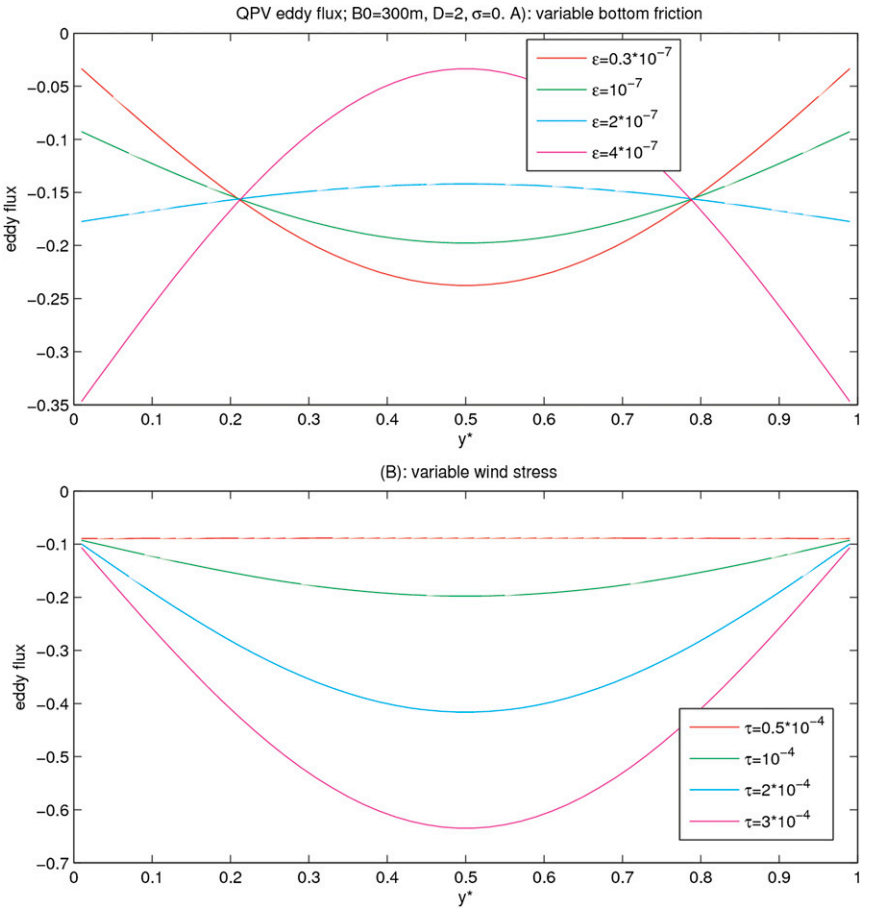

FIG. 7. QPV total eddy flux for (a) variable bottom friction with $B_0 = 300$ m, $D = 2$, and $\sigma = 0$ and (b) variable wind stress.

Figure 6b, for example, shows that even topography as small as 1–10 m already has a marked impact. In the center of the jet the eddy flux is positive for $B_0 = 1$ m and at the flanks it is negative. This distribution is similar to the flat bottom case, but the integral of the eddy flux is negative. If B_0 exceeds a value of about 10 m, the fluxes become negative at any point and reach the maximum (by modulus) at the center of the channel. The type of the curve of the eddy flux is changed from concave (which pertains to the flat bottom case) to convex (which pertains to the variable bottom topography channel). Such a change occurs in the range of amplitude of bottom topography between 10 and 100 m. For high enough B_0 increasing D leads to a minor increase of the absolute value of the negative flux at the center of the channel. This result is neither obvious nor trivial because increasing D means increasing the relative importance of bottom drag. However, the increase of D is lifting the value of Re, because of the GTB, which strongly contributes to the total eddy flux of QPV. The meridional distribution of the total eddy flux of QPV is sensitive to the bottom friction (Fig. 7a). If the coefficient of the bottom friction increases between 1.0 and $2.0 \times 10^{-7}\,\mathrm{s}^{-1}$ the type of the curve of the total eddy flux changes from convex to concave (see Fig. 7a). However, the flux does not change its sign and the meridional integral of the flux demonstrates only minor variability for fixed topography. Increasing the bottom friction from 0.3 to $4 \times 10^{-7}\,\mathrm{s}^{-1}$ yields a change (decreasing) of eddy fluxes of only 7%. This occurs because the main balance is between the wind stress and the BFS (which is equal to the total eddy flux of the QPV), whereas the bottom friction contribution plays a smaller role [see Eq. (21)].

Eddy fluxes for small wind stress are almost constant across the channel. However, they tend to a sinusoidal distribution and increase in amplitude when the amplitude of wind stress τ_0 increases. This can be anticipated because the eddy QPV fluxes in the upper layer must be proportional to τ_x by Eq. (10), while in the lower layer they must balance the viscous bottom drag by Eq. (11). As the amplitude of wind stress τ_0 increases, the dimensional bottom form stress increases to balance it,

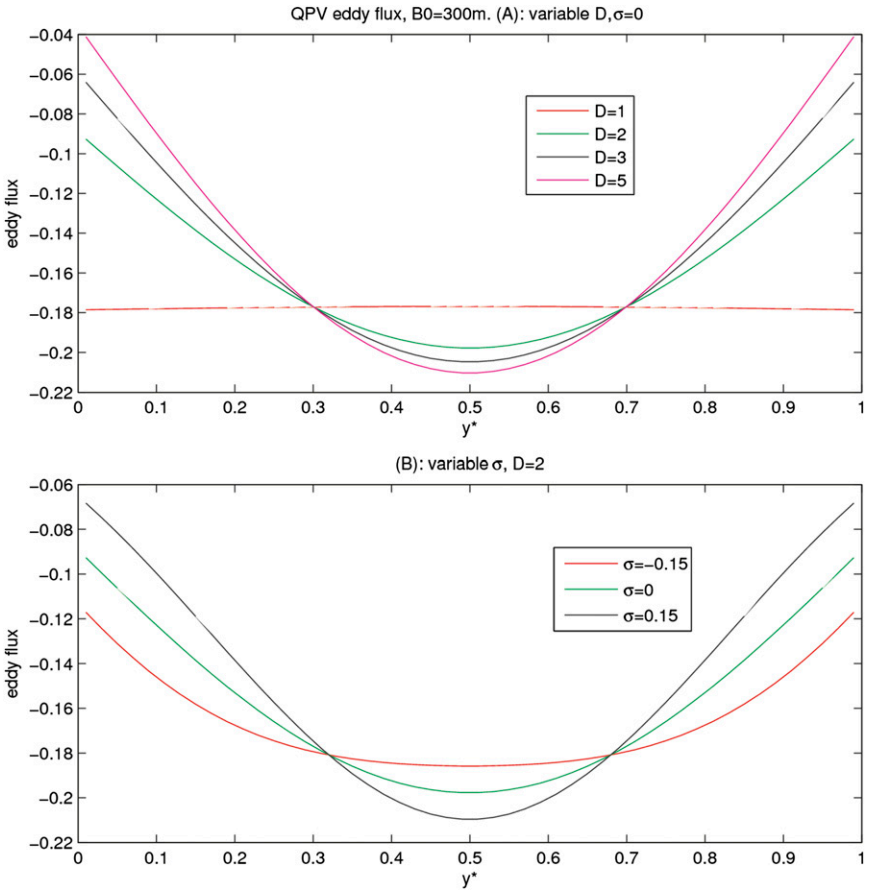

FIG. 8. QPV total eddy flux with $B_0 = 300$ m for (a) variable D and $\sigma = 0$, and (b) variable σ and $D = 2$.

while the bottom drag remains relatively small. The total eddy QPV flux becomes dominated by the upper-layer QPV flux, whose profile resembles that of the wind stress (Fig. 7b).

Eddy fluxes for small D are almost constant across the channel (Fig. 8a). However, increasing D yields redistribution of eddy fluxes, increasing (by modulus) in the center of the channel, but decreasing on the flanks. This happens because the relative importance of the eddy fluxes in the lower and upper layers is proportional to the Re/D, and since Re is a linear function of D from the GTB, their ratio is inversely proportional to D, and this means that the total eddy flux becomes dominated by the upper-layer eddy flux of QPV, whose profile resembles the wind stress [see Eq. (10)].

The geometric parameter σ contributes to the total eddy QPV flux through the term proportional to $\sigma\cos(2\pi y^*)$, which is positive for negative σ at the center of the channel. Because in the total eddy fluxes the upper-layer contribution is dominant and negative, this means reduction in the amplitude in the center of the channel compared to the case $\sigma > 0$ (Fig. 8b).

b. *Zonal transport*

Deriving an expression for the total transport of the Antarctic Circumpolar Current is a challenging task for the dynamics of the Southern Ocean. Its difficulty hinges on the need to properly address the penetration of momentum downward and its balance with the bottom form stress. Both processes are mediated by eddies and using an unsatisfactory parameterization would yield incorrect velocities and unreasonable transport.

Using our results for zonal velocities [Eqs. (A15)–(A18)], we can calculate the zonal transport. We can write the following expression for the transport T in dimensional form:

$$T = LHu_c\left(\frac{2\delta_1^2\mathrm{Re}}{\pi^2} + \frac{2\delta_1\mathrm{Re}}{\delta_2\pi^2 D} - \delta_1^2 - \frac{1}{\delta_2 D}\right). \quad (55)$$

According to this expression, the transport appears to depend on both parameters Re and D, but one of them can be eliminated by using the GTB. Substituting Re as a function of D from Eq. (37) yields

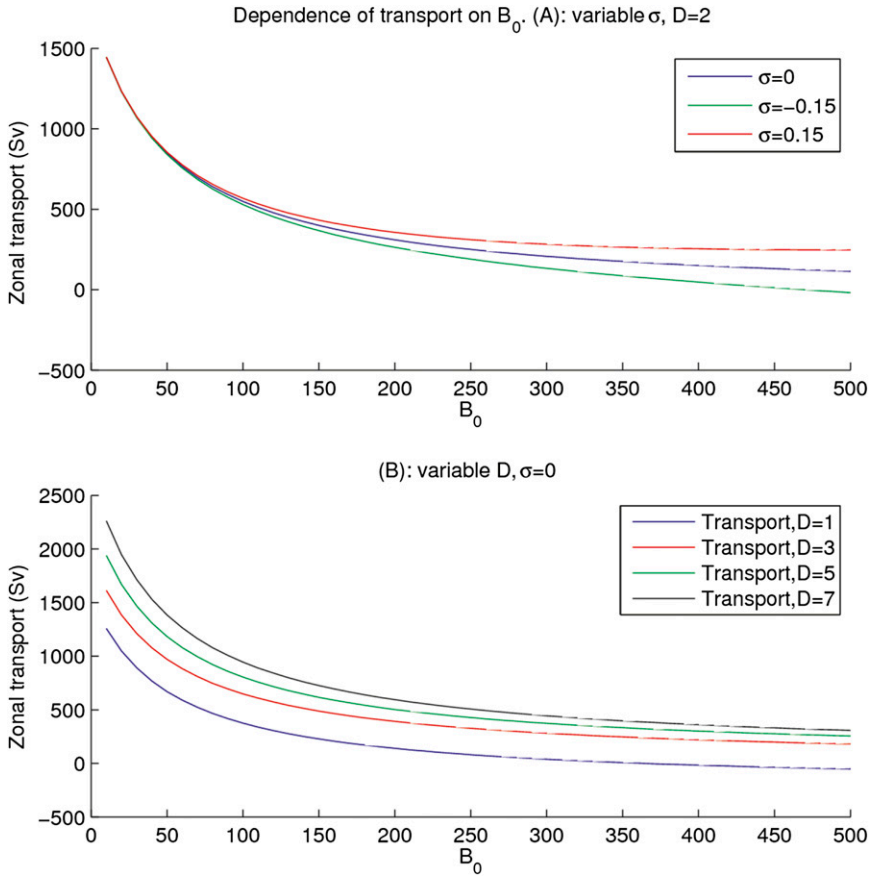

FIG. 9. Dependence of zonal transport on B_0 for (a) variable σ and $D = 2$, and (b) variable D and $\sigma = 0$.

$$T = LHu_c\left[\left(\frac{2\delta_1}{\pi^2}+\frac{2}{\delta_2\pi^2 D}\right)\left(\frac{3D}{2\alpha_B\alpha_T\alpha_U+3\alpha_B\alpha_U}+\frac{6\pi^2+3\pi^2\alpha_T+3\sigma\pi^3\delta_2\alpha_R\alpha_T}{8\alpha_T+12}\right)-\delta_1^2-\frac{1}{\delta_2 D}\right]. \quad (56)$$

Equation (56) predicts an inversely proportional dependence of the transport on the amplitude of bottom topography B_0 (see Fig. 9a). Increasing the prescribed parameter D results in an increased total transport (see Fig. 9b). This result is not obvious because D is proportional to the bottom friction. The BFS is inversely proportional to D [see Eq. (44)], and increasing D implies a decrease in the major term opposing the wind (i.e., BFS). Also, according to Eq. (56), the transport can be split into three terms: a term linearly increasing with D, a term independent of D, and a term inversely proportional to D. Their sum is increasing with D. Note that the term proportional to D in Eq. (56) is

$$T_1 = LHu_c\frac{6\delta_1}{\pi^2\alpha_B\alpha_U(2\alpha_T+3)}D.$$

It is inversely proportional to the parameter α_U, which is proportional to the bottom viscosity ϵ. The term D/α_U is independent of ϵ, and the term T_1 depends on ϵ only via α_T. Increasing ϵ makes α_T smaller. The total transport quickly decreases with increasing B_0. There is a linear relationship between the transport and parameter σ (not shown). This parameter can strongly affect the transport as B_0 is varied, especially if B_0 is high (see Fig. 9a). Note that the transport depends on the topographic parameter α_R only if the zonal average of the bottom topography deviation is not zero ($\sigma \neq 0$).

The stationary total zonal transport was calculated for fixed $D = 2$, which corresponds to a value of the CPV in the lower layer $K_2 = 500\,\mathrm{m^2\,s^{-1}}$. The coefficient in the upper layer has been calculated by using the GTB. The transport in the flat bottom case reaches an unrealistically high value of 1744 Sverdrups (Sv; $1\,\mathrm{Sv} \equiv 10^6\,\mathrm{m^3\,s^{-1}}$) with the value of $K_1 = 322.6\,\mathrm{m^2\,s^{-1}}$.

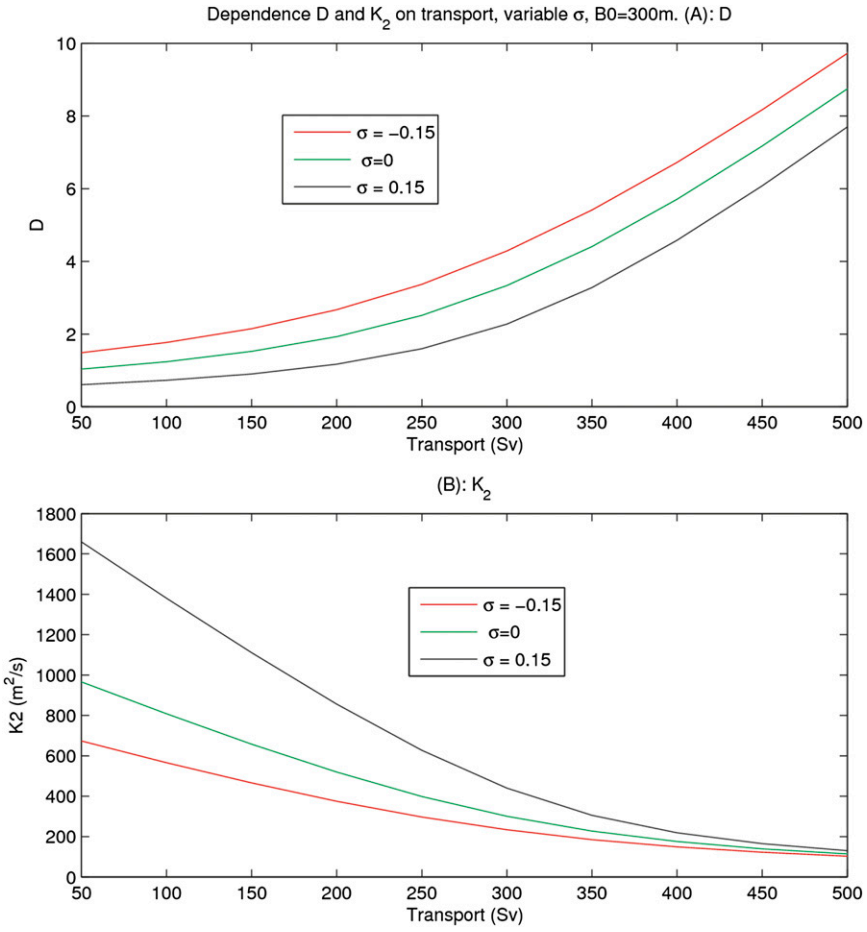

FIG. 10. Dependence of D and K_2 on transport with variable σ and $B_0 = 300$m for (a) D and (b) K_2.

The CPV in the upper layer is smaller than that in the lower layer, which agrees with Marshall (1981). The transport with variable bottom topography drops down drastically, depending on B_0. The CPV in the upper layer strongly increases compared to the flat bottom channel and is higher than the value of K_2. This coefficient decreases linearly when the parameter σ increases.

It is of interest to estimate the range of values of the CPV in the lower layer and the parameter D. The term D increases when transport increases (for fixed B_0) (see Fig. 10a). However, the value of D only increases slightly for small transports, but after about 250 Sv their increase is more substantial.

It is possible to evaluate the CPV for the fixed B_0 and variable transport from Eq. (56). The value K_2 decreases nonlinearly with increasing transport (see Fig. 10b). For $B_0 = 300$ m and $\sigma = 0$, coefficient K_2 decreases from about $970\,\mathrm{m^2\,s^{-1}}$ to about $115\,\mathrm{m^2\,s^{-1}}$. For small transports the values of K_2 vary strongly for different σ, but for transport more than about 350 Sv they are close to each other.

The zonal transport increases linearly with the wind stress (Fig. 11a). For a fixed CPV in the lower layer ($K_2 = 500\,\mathrm{m^2\,s^{-1}}$), the coefficient K_1 increases nonlinearly with wind stress (Fig. 11a). There is only weak sensitivity of the total transport to the bottom friction (Fig. 11b), which is not surprising since the main balance for wind stress is provided by inviscid BFS. The increase in Re yields an increase of transport for the same ϵ (Fig. 11b).

6. Numerical model and experiments with the eddy-resolving model

Since our analytical treatment relates to the time- and zonal-mean model with parameterized fluxes, we carry out numerical simulations with a full two-layer model to illustrate the predictions of the analytical model. We do not deal with parameterizations here, but concentrate

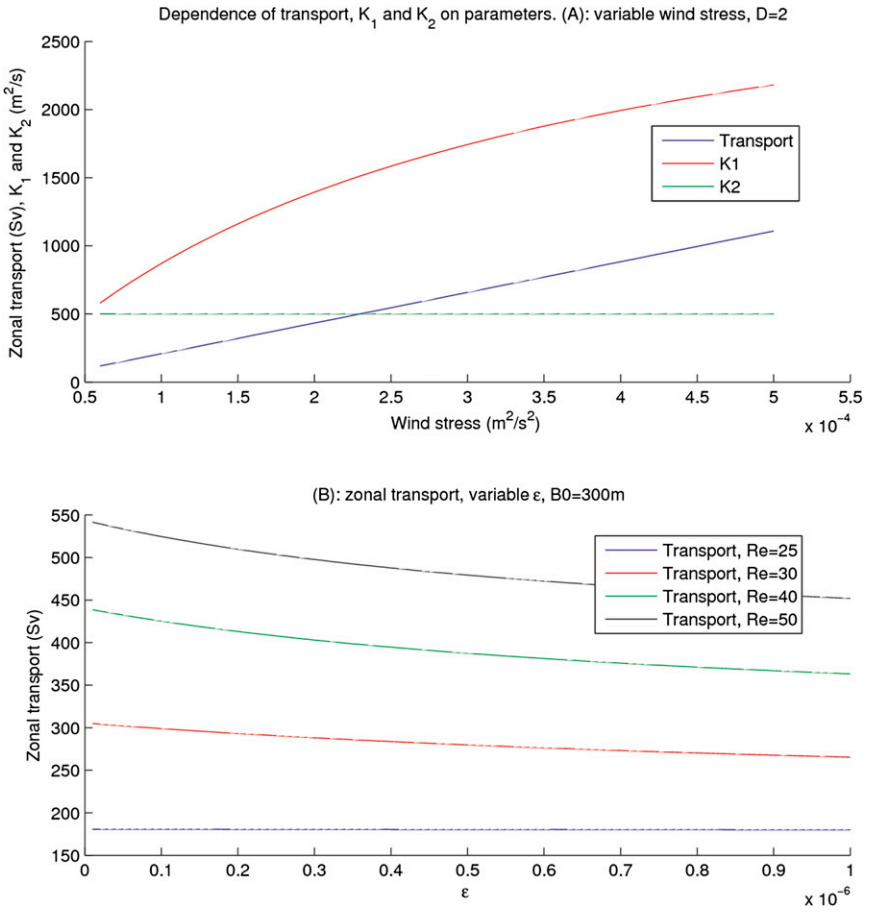

FIG. 11. Dependence of transport, K_1 and K_2 on parameters for (a) variable wind stress, with $D = 2$, and (b) variable ϵ.

on eddy fluxes in the presence of topography and show that they behave rather similarly to the predictions of the analytical model, showing also rather similar sensitivity to the governing parameters. We limit ourselves to a qualitative comparison because the analytical results above are obtained for constant K_1 and K_2, while numerical fluxes do not obey Eq. (9) with constant CPV.

The numerical model is implemented on a C grid and uses the Arakawa Jacobian (Arakawa 1966) preserving both energy and enstrophy. The time stepping and implementation of boundary conditions may introduce small nonconservative effects. The boundary conditions for the streamfunctions follow the implementation of McWilliams (1977) and McWilliams et al. (1978). The computational mesh is 800 by 150 points with $dx = dy =$ 10 km. Cyclic boundary conditions are applied in the zonal direction. On solid walls we require that $\partial^2\Psi_i/\partial y^2 = 0$ (free slip) and that $\nabla^4\Psi_i = 0$ (additional boundary condition required for biharmonic viscosity). Time stepping follows the third-order Adams–Bashforth method. The parameters are selected so as to be in agreement with the analytical model; in particular, the bottom topography is given by Eq. (26). All simulations are run for 20 years, and the results are averaged over the last 10 years. It takes a model about 10 years to reach a quasi-stationary level of energy. Although the next 10-yr period is still insufficient to reach truly stationary statistics, the deviations are already rather moderate for the eddy fluxes. The runs have been performed for three amplitudes of topography: 100, 300, and 500 m. For each of them, we run for three values of parameter $\sigma = -0.15$, 0, and 0.15 and three values of bottom drag coefficient corresponding to the inverse of 30, 115, and 360 days (high, standard, and low friction).

Figures 12 and 13 illustrate the behavior of the time- and zonal-mean meridional eddy QPV flux and the form stress for different ϵ, but fixed $\sigma = 0.15$ and for different σ and fixed $\epsilon = 10^{-7}\,\mathrm{s}^{-1}$ (standard friction), respectively. According to Eq. (10), the zonal-mean meridional PV flux in the upper layer should repeat the wind profile, and numerical simulations for the upper layer show this, as the lateral viscosity contribution is rather small, with

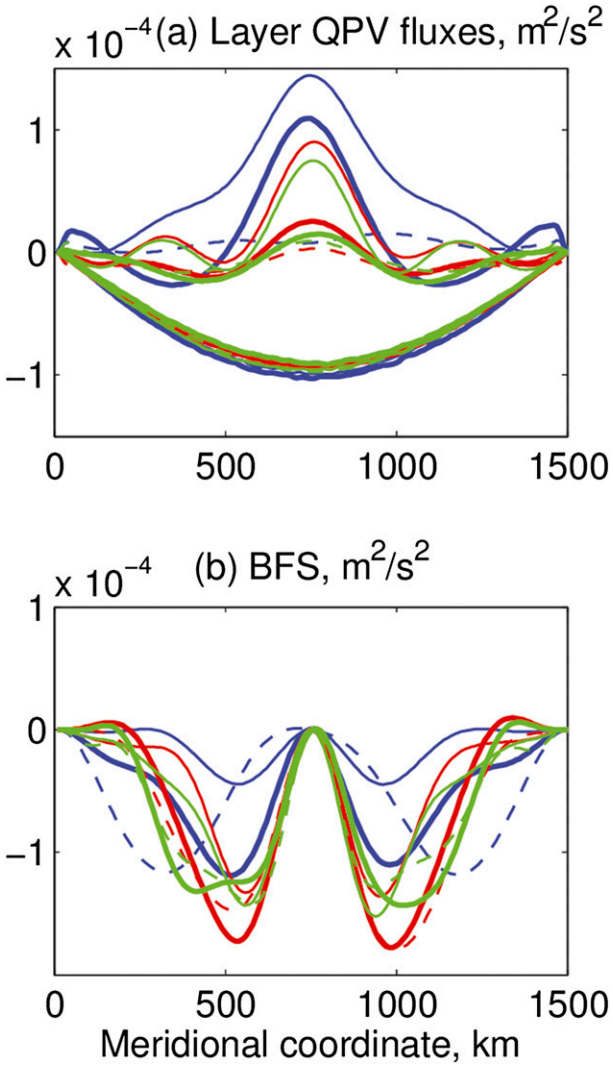

FIG. 12. Dependence of time- and zonal-mean eddy (a) QPV fluxes $\overline{q_i' v_i'} H_i$ and the (b) BFS on the meridional coordinate for various amplitudes of topography [100 m (blue), 300 m (red), and 500 m (green)] and bottom drag $\epsilon = 1/115$ (thick lines), $1/30$ (thin lines), and $1/360$ (thin dashed lines) day^{-1} from the numerical eddy-resolving experiment. The flux in the upper layer is defined by wind, so all curves collapse to the same negative sine profile. High friction (thin curves) makes the eddy flux in the lower layer more positive, that is, closer to the flat bottom situation. The case with the smallest friction and topography deviations (dashed blue) shows strong oscillations in the jet position, and the curves for it are based on a longer integration.

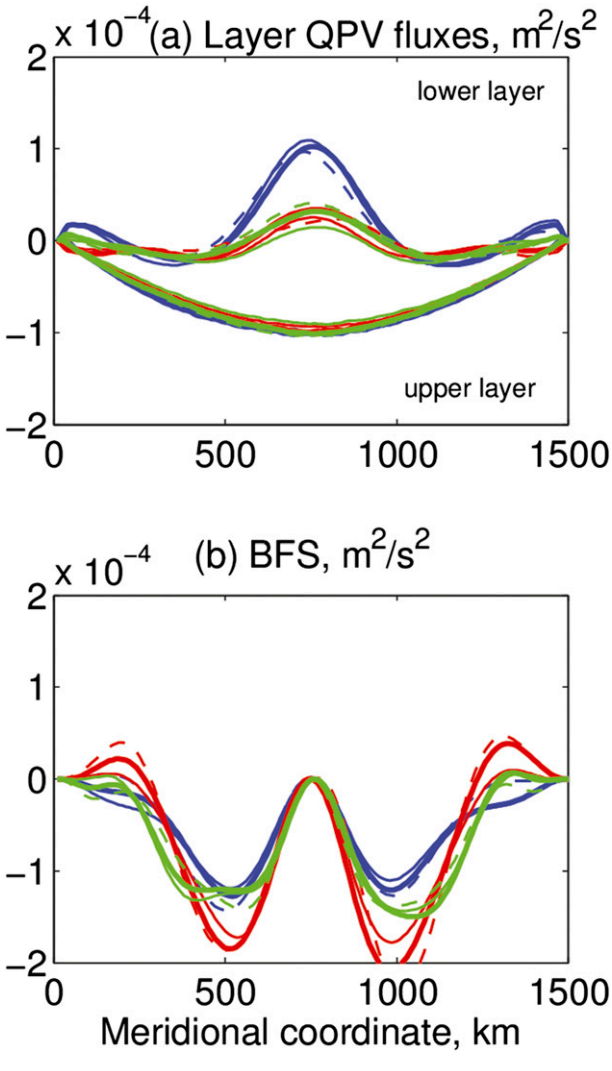

FIG. 13. As in Fig. 12, but for the parameter $\sigma = 0.15$ (thin lines), 0 (thick lines), and -0.15 (thin dashed lines). Variable σ leads to some spread, but longer averaging is needed to estimate its effect reliably.

some spread due to insufficiently long averaging time. The eddy flux in the lower layer, however, is modified by the presence of topography and becomes progressively more negative and loses its amplitude as the amplitude of the bottom topography B_0 is increased. This modification is compensated by the BFS, and the GTB is maintained with a very high accuracy. Note that the compensation of eddy flux with the BFS is not local, but involves redistribution of flux even in this zonal-mean picture.

According to Fig. 13, varying σ in the selected range leads to relatively small changes. Variations in the bottom drag coefficient modify the balance to a larger extent, as follows from Fig. 12. The low bottom drag corresponds to a more barotropic flow, with larger velocities in the lower layer, and more negative mean meridional QPV flux. In general, an increase in the topographic amplitude and a reduction in bottom drag have similar impact on the fluxes.

This time- and zonal-mean picture is very different from the 2D patterns of time-mean fluxes. The latter are

dominated by large rotational contributions associated with the topography. For this reason, we did not attempt to fit the simulated fluxes with Eq. (9).

We note however, that the change in the role of BFS as σ and ϵ are varied is similar to that derived analytically. The contribution from BFS in the GTB increases in absolute value with reduction in ϵ and increase in the topographic amplitude, as could be expected. The sensitivity to friction is the largest for small topographic variations and shows a tendency to saturation as B_0 is increased. Variations in σ lead to small changes in the BFS contribution on the level of several percent. Discussing them would require much longer averaging.

7. Summary and discussion

Both the energy inequality and generalized theorem of Bretherton impose strong restrictions on the eddy PV transfer coefficients. If the chosen CPVs fail to satisfy these constraints, the resulting equations violate the basic laws of energy or momentum conservation.

We explore this issue in an elementary way, taking time- and zonal-mean QG two-layer equations, parameterizing the eddy PV fluxes as downgradient (with constant layer diffusivities), solving the equations, and analyzing the limitations on the diffusivities (CPVs).

We demonstrate that the bottom topography plays an important role in these restrictions, especially for momentum. It explicitly enters the GTB, which should be satisfied by solutions with parameterized QPV fluxes. Any failure to do so leads to violation of the major momentum balance in zonal flows (like the ACC) between the wind stress and the bottom form stress (Munk and Palmén 1951; Ivchenko et al. 1996; Stevens and Ivchenko 1997).

The energy inequality requires that the parameter Re must be greater than the critical value $\mathrm{Re}_{\mathrm{cr}} = 4$, which means that the CPV in the upper layer (main thermocline) must be less than a certain critical value, depending on the amplitude of the wind stress, the layer thickness, and the planetary vorticity gradient β, for any type of bottom topography or flat bottom case. For the standard set of parameters this value is $K_1 < 5.6 \times 10^3\,\mathrm{m^2\,s^{-1}}$.

Because of these restrictions, the parameterization for eddy PV fluxes allows only limited freedom in the choice of coefficients. If we select the value for the coefficient K_1 in the upper layer (which has to comply with the EI), the value of the coefficient in the lower layer K_2 is then prescribed by the GTB. We found a linear relationship between D and Re set by the GTB, which is nonlinear between K_1 and K_2. The link between the coefficients (or parameters Re and D) strongly depends on bottom topography, that is, on its amplitude, zonal, and meridional variability. For flat bottom topography, the GTB requires that the parameter $\mathrm{Re} > \pi^2(2\delta_1)^{-1}$. The values of $\mathrm{Re}_{\mathrm{cr}}$ for variable bottom topography and the slope of the line $D(\mathrm{Re})$ are strongly dependent on the parameters of bottom topography. For example, changing the mean zonal average value of topography (the parameter σ in the case considered) shifts the value of $\mathrm{Re}_{\mathrm{cr}}$. If D is fixed, the parameter Re has a nonlinear dependence on B_0 (decreasing), but remains higher than $\mathrm{Re}_{\mathrm{cr}}$; for B_0 in the range between 10 and 500 m, the range of Re is within a factor of 3 of its lowest value. The CPV in the upper layer is larger than in the lower layer; the dependence of K_1 on the amplitude of the bottom topography is nonlinear, but it increases for higher values of B_0. For the topography considered here, the value of K_1 (for K_2 fixed) substantially depends on the meridional gradient of zonally averaged bottom topography. The bottom form stress shows a strong nonlinear dependence on the amplitude of the bottom topography for not very high values of B_0, less than about 100 m.

The analytical solution developed here allows us to emphasize the importance of the GTB. For example, it shows that increasing the parameter D leads to an increase of the magnitude of the total eddy flux, which is not immediately apparent (why should a higher bottom friction yield a higher eddy flux?). The relative importance of the eddy fluxes in the lower and upper layers is proportional to Re/D, and since Re is a linear function of D from the GTB, their ratio is inversely proportional to D, and this means that the total eddy flux becomes dominated by the upper-layer eddy flux of QPV.

The solution also allows one to calculate the total zonal transport as a function of external parameters and of diffusivities (or one of Re and D) that should be chosen from observation or numerical simulations. It is rather sensitive to the amplitude of bottom topography, which drastically reduces the transport from unrealistically high values for the flat bottom case to plausible values even for moderately large B_0.

Admittedly, the approach taken here is a simplification and with just two layerwise constant QPV diffusivities the constraint provided by the GTB is much more restrictive than it would be for many layers, leaving alone the limitations of the quasigeostrophic approximation. However, we would like to stress that while the presence of constraints is well recognized, the fact that they are affected by bottom topography is mentioned less frequently. We see the results presented here as posing the question about the implications of these constraints for more realistic, primitive equation models, which would be of great interest to explore.

Acknowledgments. We are grateful to two anonymous reviewers for their insightful and detailed comments that led to a greatly improved manuscript. One of them has drawn our attention to the study of Taylor (1915) used in developing the Bretherton theorem. The other reviewer proposed the explanation of the increase in eddy QPV flux when the amplitude of wind stress increases.

APPENDIX

Asymptotic Solutions

Expressions for meridional gradients of QPV are obtained by taking the time and zonal average of the potential vorticity [Eqs. (3)–(4)] and then differentiating with respect to y. In nondimensional form these are

$$\frac{\partial q_1^*}{\partial y^*} = -\frac{\gamma^2}{\delta_1\delta_2}\frac{\partial^2 u_1^*}{\partial y^{*2}} + 1 + \frac{1}{\delta_1}(u_1^* - u_2^*) \quad \text{and} \quad \text{(A1)}$$

$$\frac{\partial q_2^*}{\partial y^*} = -\frac{\gamma^2}{\delta_1\delta_2}\frac{\partial^2 u_2^*}{\partial y^{*2}} + 1 - \frac{1}{\delta_2}(u_1^* - u_2^*) - 2\pi\alpha_R\sigma\cos(2\pi y^*), \quad \text{(A2)}$$

where $\alpha_R = (|f_0|B_0)(LH_2\beta)^{-1}$ is the dimensionless parameter that measures the ratio between the topographic, that is, $(|f_0|B_0)H_2^{-1}$ and planetary βL contributions to the QPV in the lower layer.

The boundary conditions [Eq. (29)] in nondimensional parameterized form, using Eq. (9), yields

$$\left(s_i\frac{\partial q_i^*}{\partial y^*}\right)\Bigg|_{0,1} = 0. \quad \text{(A3)}$$

One cannot expect the PV gradients on the walls to be zero, since in that case a large planetary PV gradient would require unphysically large gradients of the relative vorticity. So we have to require zero values of CPV on the walls. Coefficients s_i (CPV) are free parameters, and as the first step we consider them to be constant in each layer almost everywhere except the thin boundary layers near walls ($\Delta \ll 1$), where we assume them to be proportional to the distance to the wall:

$$s_1 = \begin{cases} r = \text{const}\ \Delta \le y^* \le 1-\Delta \\ r\dfrac{y^*}{\Delta}\ 0 \le y^* \le \Delta \\ r\dfrac{(1-y^*)}{\Delta}\ (1-\Delta) \le y^* \le 1 \end{cases}. \quad \text{(A4)}$$

The coefficient of diffusivity in the lower layer s_2 is $s_2 = \Theta s_1$ at any point, $0 \le y^* \le 1$. The term Θ must be found from integral constraint (16).

We set the time-averaged streamfunctions Ψ_i and corresponding velocities in the form of a product of a meridionally varying function $Q(y)$ and a zonally varying Fourier series:

$$\Psi_i(x,y) = Q(y)\left[1 + \sum_{l=1}^{2N} a_l \sin(l\pi x L_x^{-1}) + \sum_{l=1}^{2N} b_l \cos(l\pi x L_x^{-1})\right]. \quad \text{(A5)}$$

To satisfy zonal periodicity (i.e., $\Psi_i|_0 = \Psi_i|_{L_x}$), the odd modes have to be excluded, that is

$$\Psi_i(x,y) = \overline{\Psi_i}(y)\left[1 + \sum_{l=2}^{2N} a_l \sin(l\pi x L_x^{-1}) + \sum_{l=2}^{2N} b_l \cos(l\pi x L_x^{-1})\right], \quad \text{(A6)}$$

where l is constrained to be even. If this expression is substituted into Eq. (30) most of the components will have zero contribution; the only nonzero component corresponds to $l = 2k$ (i.e., the wavenumber of the topography), therefore we use $b = b_{2k}$. Note that $Q(y)$ is equal to the zonal-averaged value $\overline{\Psi_i}(y)$.

The nondimensional QPV [Eqs. (27)–(28)] for $\Delta \le y^* \le 1 - \Delta$ (i.e., away from the thin boundary layers) can be rewritten in the following form:

$$\frac{1}{\mathrm{Re}}\frac{d^2 q_1^*}{dy^{*2}} - \cos(\pi y^*) = 0 \quad \text{and} \quad \text{(A7)}$$

$$\frac{1}{D}\frac{d^2 q_2^*}{dy^{*2}} + \frac{du_2^*}{dy^*} = 0, \quad \text{(A8)}$$

where $\mathrm{Re} = (u_s L)K_1^{-1}$ and $D = (\epsilon u_c)(\beta K_2)^{-1}$ are the nondimensional parameters [see details after Eq. (32)].

Eq. (A7) represents the main dynamical balance in the upper layer, where the external forcing (curl of wind stress) is balanced by the eddy fluxes of the QPV. Eq. (A8) is the main dynamical balance for the lower layer, where the eddy fluxes of the QPV are balanced by bottom friction.

Equations similar to Eqs. (A7)–(A8) can be written for the southern and northern boundary layers, that is, for the southern boundary, $0 \le y^* < \Delta$:

$$\frac{d}{dy^*}\left(y^*\frac{dq_1^*}{dy^*}\right) - \mathrm{Re}\,\Delta\cos(\pi y^*) = 0 \quad \text{and} \tag{A9}$$

$$\frac{d}{dy^*}\left(y^*\frac{dq_2^*}{dy^*}\right) + D\Delta\frac{du_2^*}{dy^*} = 0. \tag{A10}$$

Similar equations can be written for the boundary layer near the northern wall, that is, $1 - \Delta < y^* \le 1$ (not shown).

The system of equations is solved with boundary conditions that match QPV fluxes and velocities at the boundaries of the regions, that is, at $y^* = \Delta, 1 - \Delta$. As the forcing at the walls goes to zero, then

$$u_i^*|_{0,1} = 0, \tag{A11}$$

(see Marshall 1981).

Our system has a small parameter γ, which characterizes the ratio of the Rossby deformation radius to the channel width. Substituting Eqs. (A1)–(A2) into Eqs. (A7)–(A10), one obtains a system of equations with a small parameter at the highest derivative. Also in the equation for the lower layer there are regular singularities at the points $y^* = 0$ and 1. To solve the system we use an asymptotic expansion by a small parameter and to eliminate difficulties related to regular singularities we use a Frobenius method (Nayfeh 1973; Ivchenko et al. 1997), which is an asymptotic expansion in power series in the vicinity of regular singularities. We present u_i^* in the form of the following asymptotic series:

$$\begin{aligned} u_i^*(y^*) = {} & u_i^{(0)}(y^*) + \gamma u_i^{(1)}(y^*) + \gamma^2 u_i^{(2)}(y^*) + \cdots \\ & + \widetilde{u}_i^{(0)}(\zeta) + \gamma\widetilde{u}_i^{(1)}(\zeta) + \gamma^2\widetilde{u}_i^{(2)}(\zeta) + \cdots \\ & + \widetilde{\widetilde{u}}_i^{(0)}(\xi) + \gamma\widetilde{\widetilde{u}}_i^{(1)}(\xi) + \gamma^2\widetilde{\widetilde{u}}_i^{(2)}(\xi) + \cdots . \end{aligned} \tag{A12}$$

Here, ζ and ξ are "stretched coordinates"; $\zeta = y^*\gamma^{-1}$ and $\xi = (1 - y^*)\gamma^{-1}$; $u_i^{(j)}(y^*)$ is a basic system of functions; and $\widetilde{u}_i^{(j)}(\zeta)$ and $\widetilde{\widetilde{u}}_i^{(j)}(\xi)$ are a system of "correction functions," which are important only near the walls and exponentially decreasing with distance; that is,

$$\widetilde{u}_i^{(j)}(\zeta) \to 0, \quad \text{as} \quad \zeta \to \infty \quad \text{and} \tag{A13}$$

$$\widetilde{\widetilde{u}}_i^{(j)}(\xi) \to 0, \quad \text{as} \quad \xi \to \infty. \tag{A14}$$

The asymptotic solutions for the mean zonal velocities away from the boundaries, $\Delta \le y^* \le (1 - \Delta)$, are

$$\begin{aligned} u_1^* = {} & \left[\frac{\mathrm{Re}\delta_1}{\pi} + \frac{\mathrm{Re}\delta_1}{D\delta_2\pi}\right]\sin(\pi y^*) - \delta_1 - \frac{1}{D\delta_2} \\ & + \frac{2\pi\alpha_R\sigma}{D}\cos(2\pi y^*) + O(\gamma^2) \quad \text{and} \end{aligned} \tag{A15}$$

$$u_2^* = \frac{\mathrm{Re}\delta_1}{D\delta_2\pi}\sin(\pi y^*) - \frac{1}{D\delta_2} + \frac{2\pi\alpha_R\sigma}{D}\cos(2\pi y^*) + O(\gamma^2). \tag{A16}$$

The asymptotic solutions for the mean zonal velocity in the southern thin boundary layer $0 \le y^* < \Delta$ can be written as

$$\begin{aligned} u_1^* = {} & (\mathrm{Re}\Delta\delta_1 - \delta_1)[1 - \exp(-\sqrt{\delta}_2\zeta)] + \frac{y^*}{D\Delta\delta_2}[(\mathrm{Re}\Delta\delta_1 - 1) + 2\pi\delta_2\alpha_R\sigma\cos(2\pi y^*)] \\ & - \gamma\left[\frac{(\mathrm{Re}\Delta\delta_1 - \delta_1)}{4D\Delta\delta_2}\zeta\exp(-\sqrt{\delta}_2\zeta)\right] - \gamma\left[\frac{(\mathrm{Re}\Delta\delta_1 - \delta_1)}{4D\Delta\sqrt{\delta}_2}\zeta^2\exp(-\sqrt{\delta}_2\zeta)\right] + O(\gamma^2), \quad \text{and} \end{aligned} \tag{A17}$$

$$u_2^* = \frac{y^*}{D\Delta\delta_2}[(\mathrm{Re}\Delta\delta_1 - 1) + 2\pi\delta_2\alpha_R\sigma\cos(2\pi y^*)] - \gamma\frac{(\mathrm{Re}\Delta\delta_1 - \delta_1)}{D\Delta\delta_2}\zeta\exp(-\sqrt{\delta}_2\zeta) + O(\gamma^2). \tag{A18}$$

Similar solutions can easily be obtained for the northern thin boundary layer $1 - \Delta < y^* \le 1$.

Note that in the rhs of Eqs. (A15)–(A18) there are now the terms proportional σ, which were not present in the case with zero value of the zonally averaged bottom topography (Ivchenko et al. 2013).

REFERENCES

Arakawa, A., 1966: Computational design for long-term numerical integration of the equations of fluid motion: Two-dimensional incompressible flow. Part 1. *J. Comput. Phys.,* **1,** 119–143.

Bretherton, F. S., 1966: Critical layer instability in baroclinic flows. *Quart. J. Roy. Meteor. Soc.,* **92,** 325–334.

Delworth, T. L., and Coauthors, 2012: Simulated climate and climate change in the GFDL CM2.5 high-resolution coupled climate model. *J. Climate,* **25,** 2755–2781.

Eden, C., 2010: Parameterising meso-scale eddy momentum fluxes based on potential vorticity mixing and a gauge term. *Ocean Modell.,* **32,** 58–71.

——, and R. J. Greatbatch, 2008: Towards a mesoscale eddy closure. *Ocean Modell.,* **20,** 223–239.

Fox-Kemper, B., R. Ferrari, and J. Pedlosky, 2003: On the indeterminacy of rotational and divergent eddy fluxes. *J. Phys. Oceanogr.,* **33,** 478–483.

Green, J. S. A., 1970: Transfer properties of the large-scale eddies and the general circulation of the atmosphere. *Quart. J. Roy. Meteor. Soc.,* **96,** 157–185.

Harrison, D. E., 1978: On the diffusion parameterization of mesoscale eddy effects from a numerical ocean experiment. *J. Phys. Oceanogr.,* **8,** 913–918.

Ivchenko, V. O., 1984: Parameterization of the eddy fluxes of the quasi-geostrophic potential vorticity in zonal flows. *Dokl. Akad. Nauk SSSR,* **277,** 972–976.

——, 1987: Influence of bottom topography on the eddy transfer coefficient. *Izv. Akad. Nauk SSSR, Atmos. Ocean Phys.,* **23,** 200–208.

——, K. J. Richards, and D. P. Stevens, 1996: The dynamics of the Antarctic Circumpolar Current. *J. Phys. Oceanogr.,* **26,** 753–774.

——, ——, B. Sinha, and J.-O. Wolff, 1997: Parameterization of mesoscale eddy fluxes in zonal ocean flows. *J. Mar. Res.,* **55,** 1127–1162.

——, S. Danilov, and D. Olbers, 2008: Eddies in numerical models of the Southern Ocean. *Ocean Modeling in an Eddying Regime, Geophys. Monogr.,* Vol. 177, Amer. Geophys. Union, 177–198.

——, B. Sinha, V. B. Zalesny, R. Marsh, and A. T. Blaker, 2013: Influence of bottom topography on integral constraints in zonal flows with parameterized potential vorticity fluxes. *J. Phys. Oceanogr.,* **43,** 311–323.

Kamenkovich, V. M., M. N. Koshlyakov, and A. S. Monin, 1986: *Synoptic Eddies in the Ocean.* D. Reidel Publishing Company, 433 pp.

Killworth, P. D., 1997: On the parameterization of eddy transfer. Part 1. Theory. *J. Mar. Res.,* **55,** 1171–1197.

Marshall, D. P., and A. J. Adcroft, 2010: Parameterization of ocean eddies: Potential vorticity mixing, energetics and Arnold's first stability theorem. *Ocean Modell.,* **32,** 188–204.

——, J. R. Maddison, and P. S. Berloff, 2012: A framework for parameterizing eddy potential vorticity fluxes. *J. Phys. Oceanogr.,* **42,** 539–557.

Marshall, J. C., 1981: On the parameterization of geostrophic eddies in the ocean. *J. Phys. Oceanogr.,* **11,** 257–271.

McWilliams, J. C., 1977: A note on a consistent quasigeostrophic model in a multiply connected domain. *Dyn. Atmos. Oceans,* **1,** 427–441.

——, W. R. Holland, and J. S. Chow, 1978: A description of numerical Antarctic Circumpolar Currents. *Dyn. Atmos. Oceans,* **2,** 213–291.

Munk, W. H., and E. Palmén, 1951: Note on the dynamics of the Antarctic Circumpolar Current. *Tellus,* **3,** 53–55.

Nayfeh, A. H., 1973: *Perturbation Methods.* Wiley-Interscience, 437 pp.

Olbers, D., 2005: On the role of eddy mixing in the transport of zonal ocean currents. *Marine Turbulence: Theories, Observations, and Models,* H. Baumert, J. Simpson, and J. Sündermann, Eds., Cambridge University Press, 630 pp.

Pedlosky, J., 1964: The stability of currents in the atmosphere and the ocean: Part I. *J. Atmos. Sci.,* **21,** 201–219.

——, 1979: *Geophysical Fluid Dynamics.* Springer Verlag, 624 pp.

Rhines, P. B., 1977: The dynamics of unsteady currents. *The Sea—Ideas and Observations on Progress in the Study of the Seas,* E. D. Goldberg, Ed., *Marine Modeling,* Vol. 6, John Wiley and Sons, 189–318.

Ringler, T., and P. Gent, 2011: An eddy closure for potential vorticity. *Ocean Modell.,* **39,** 125–134.

Sinha, B., and K. J. Richards, 1999: Jet structure and scaling in Southern Ocean models. *J. Phys. Oceanogr.,* **29,** 1143–1155.

Stevens, D. P., and V. O. Ivchenko, 1997: The zonal momentum balance in an eddy-resolving general circulation model of the Southern Ocean. *Quart. J. Roy. Meteor. Soc.,* **123,** 929–951.

Taylor, G. I., 1915: Eddy motion in the atmosphere. *Philos. Trans. Roy. Soc. London,* **A215,** 1–26.

Treguier, A. M., and J. C. McWilliams, 1990: Topographic influences on wind-driven, stratified flow in a β-plane channel: An idealized model for the Antarctic Circumpolar Current. *J. Phys. Oceanogr.,* **20,** 321–343.

——, I. M. Held, and V. D. Larichev, 1997: Parameterization of quasigeostrophic eddies in primitive equation ocean models. *J. Phys. Oceanogr.,* **27,** 567–580.

Wardle, R., and J. Marshall, 2000: Representation of eddies in primitive equation models by a PV flux. *J. Phys. Oceanogr.,* **30,** 2481–2503.

Welander, P., 1973: Lateral friction in the ocean as an effect of potential vorticity mixing. *Geophys. Fluid Dyn.,* **5,** 173–189.

Wolff, J.-O., E. Maier-Reimer, and D. J. Olbers, 1991: Wind-driven flow over topography in a zonal β-plane channel: A quasi-geostrophic model of the Antarctic Circumpolar Current. *J. Phys. Oceanogr.,* **21,** 236–264.